

**APPENDIX C:**

**Modeling the Transport of Reactive and Non-Reactive Solutes in  
Cores from the Cannikin Test Site, Amchitka Island, Alaska**

by

N. Brown and C. Papelis  
Division of Hydrologic Sciences  
Desert Research Institute



**MODELING THE TRANSPORT OF REACTIVE AND NONREACTIVE  
SOLUTES IN CORES FROM THE CANNIKIN TEST SITE,  
AMCHITKA ISLAND, ALASKA**

*Prepared by*

**Nicole Brown and Charalambos Papelis  
Division of Hydrologic Sciences  
Desert Research Institute  
University and Community College System of Nevada**

*Prepared for*

**Nevada Operations Office  
U.S. Department of Energy  
Las Vegas, Nevada**

**September 1999**

## EXECUTIVE SUMMARY

During the period of nuclear weapons production and testing, the United States government conducted a series of nuclear weapons tests at various sites throughout the United States and its territories. The nuclear testing performed at these sites resulted in subsurface contamination from contaminants such as radionuclides (e.g., the cesium radionuclide,  $^{137}\text{Cs}$ ), organic compounds, toxic metals (such as lead, Pb), hydrocarbons, drilling mud and residues from plastics, epoxies, and drilling instrumentation (U.S. DOE, 1996). Because of their toxicity or radioactivity, many of these contaminants are considered to be major health hazards and consequently pose a threat to organisms that are exposed to them (in particular, humans and wildlife). The fate, transport, and distribution of contaminants in the subsurface environment are significantly controlled by groundwater movement and the extent of interaction between the contaminants and surrounding rock matrix. Studies have shown that a number of chemical and physical mechanisms occurring within the subsurface may cause retardation of contaminants with respect to groundwater flow.

In an effort to estimate the migration of radionuclides and toxic compounds from the Cannikin Test Site, Amchitka Island, Alaska, this project component investigated the mobility of reactive (lead and cesium) and nonreactive (bromide) solutes through core samples obtained from the Cannikin site. Lead (Pb) and cesium (Cs) were chosen because of their different reactive characteristics and because they may occur in the subsurface environment as by-products of the underground nuclear detonation that was performed at the site in November 1971. Bromide (Br) was chosen because of its nonreactive characteristics so that an assessment could be made to determine how the rate of solute transport varies between nonreactive and reactive species. Additionally, by using a nonreactive tracer, we could estimate how retardation is affected by diffusion only, since Br is not expected to sorb appreciably. Though chloride is often used as a nonreactive solute, analysis of the site's groundwater yielded a high chloride concentration (1,920-16,000 mg/L) so that the chloride ion would be an inappropriate tracer.

Experiments were conducted with Cannikin Test Site basalt and breccia core samples obtained from the U.S. Geological Survey Core Library at the Nevada Test Site. These samples were ground, characterized by a number of physiochemical methods, and subsequently used in equilibrium sorption experiments with Pb and Cs. The remaining, intact materials were used in the diffusion experiments with Br. With respect to the sorption experiments, Pb displayed a behavior typical of cation sorption on amphoteric surface sites, with fractional uptake increasing with increasing pH, despite the high ionic strength of the synthetic groundwater solution used in these experiments. Such behavior is consistent with sorption on amphoteric surface sites as opposed to internal cation exchange sites. Experiments with Cs showed no sorption in the high ionic strength synthetic groundwater. It is thus expected that at high ionic strength, Cs would be highly mobile and exhibit no significant sorption on the solid materials.

Based on the experimental sorption data, parameters describing both linear and Freundlich isotherms were estimated for a variety of conditions. The results indicate that equilibrium partitioning at the solid-water interface is strongly pH-dependent for Pb and virtually non-existent for Cs under field conditions. As a consequence, modeling the transport of these contaminants, Pb in particular, requires knowledge of or assumptions about the groundwater pH. Under certain conditions, the isotherms for Pb were approximately linear. In most cases, however, deviations from linearity suggested that the use of the Freundlich isotherm would be more appropriate to accurately model the data.

The results of the diffusion experiments using a sodium bromide (NaBr) tracer revealed two trends. First, the extent of diffusion varied significantly with respect to each sorbent. Second, the extent of diffusion and the resulting diffusion coefficient varied with time. It was found that the basalt sample generally had

lower effective diffusion coefficients than the breccia. The calculated tortuosity for the basalt (being inversely proportional to the effective diffusion coefficient) was therefore larger in all instances than the tortuosity calculated for the breccia by a factor of approximately 1.5-2.

The results of the diffusion experiments indicate that, on average, ions in solution would most likely travel faster in the breccia than in the basalt. This is somewhat expected, as the breccia has a slightly higher porosity than the basalt, thereby providing additional pathways through which ions could travel.

The parameters determined in this study can be used to reduce the uncertainty in radionuclide transport modeling by accounting for retardation of radionuclides and other contaminants of concern due to sorption on, and diffusion through, subsurface materials. Finally, it cannot be overemphasized that the results reported here are specific to the conditions used and that, given the non-linearity of some of these systems, use of these parameters outside their range of applicability might result in significant errors.

## CONTENTS

EXECUTIVE SUMMARY .....	ii
LIST OF FIGURES .....	v
LIST OF TABLES .....	vi
INTRODUCTION .....	C-1
MATERIALS AND METHODS .....	C-1
Adsorbent Characterization .....	C-1
Sorbent Mineralogy .....	C-2
Major and Trace Element Analyses .....	C-4
Particle Morphology .....	C-5
Bulk and True Density Analyses .....	C-6
Specific Surface Area and Pore Size Distribution .....	C-6
Soil Solution pH and Cation Exchange Capacity .....	C-9
The Elements of Interest .....	C-9
Lead .....	C-9
Cesium .....	C-10
Bromine .....	C-10
Experimental Procedures .....	C-10
Batch Equilibrium Sorption Experiments with the Cannikin Site Core Samples .....	C-10
Diffusion Experiments with the Cannikin Site Core Samples .....	C-12
RESULTS AND DISCUSSION .....	C-13
Sorption of Pb and Cs on Cannikin Basalt and Breccia .....	C-13
Lead Sorption .....	C-13
Cesium Sorption .....	C-16
Isotherm Parameter Estimation .....	C-16
Diffusion of Br through Cannikin Basalt and Breccia .....	C-21
Diffusion Parameter Estimation .....	C-21
Solution to the Diffusion Equation for Nonreactive Solutes .....	C-23
Bromide Diffusion .....	C-24
Diffusion Coefficients for Pb and Cs .....	C-27
SUMMARY, CONCLUSIONS, AND RECOMMENDATIONS .....	C-28
REFERENCES .....	C-30

## LIST OF FIGURES

1.	SEM image of breccia (magnification 12x).....	A1
2.	SEM/EDX image (1) of basalt .....	A2
3.	SEM/EDX image (2) of basalt .....	A3
4.	SEM/EDX image (3) of basalt .....	A4
5.	SEM/EDX image (1) of breccia .....	A5
6.	SEM/EDX image (2) of breccia .....	A6
7.	Isotherm of nitrogen adsorption/desorption on the basalt.....	C-8
8.	Isotherm of nitrogen adsorption/desorption on the breccia.....	C-8
9.	Experimental apparatus used in the diffusion experiments with NaBr.....	C-13
10.	Sorption of Pb on 1.0 g/L basalt. ....	C-14
11.	Sorption of Pb on 1.0 g/L breccia. ....	C-15
12.	Sorption of $10^{-4}$ to $10^{-6}$ M Pb on basalt and breccia.....	C-15
13.	Comparison of sorption of $10^{-4}$ to $10^{-6}$ M Pb on larger and smaller size fractions of basalt. ....	C-17
14.	Comparison of sorption of $10^{-4}$ to $10^{-6}$ M Pb on larger and smaller size fractions of breccia. ....	C-17
15.	Sorption of $1 \times 10^{-6}$ M Cs on 1.0 g/L basalt and breccia. ....	C-18
16.	Linear isotherms of $\text{Pb}(\text{NO}_3)_2$ sorption on basalt at pH values of 6,7,8, and 9.....	C-20
17.	Linear isotherms of $\text{Pb}(\text{NO}_3)_2$ sorption on breccia at pH values of 6,7,8, and 9.....	C-20
18.	Diffusion of Br out of a basalt core sample as a function of time. ....	C-25
19.	Diffusion of Br out of a breccia core sample as a function of time.....	C-25
21.	Plot of experimental results and linear regression line of Br diffusion through breccia core. ....	C-26
20.	Plot of experimental results and linear regression line of Br diffusion through basalt core. ....	C-26

## LIST OF TABLES

1a.	Major element composition of the breccia and basalt.....	C-4
1b	Trace element composition of the breccia and basalt.....	C-5
2.	Measured specific surface areas of basalt and breccia sorbents.....	C-7
3.	Pore size measurements for the basalt and breccia.....	C-7
4.	Composition of site and synthetic groundwater. ....	C-12
5.	Linear and Freundlich isotherm parameters for lead sorption. ....	C-19
6.	Diffusion parameters for Br tracer through basalt breccia.....	C-24
7.	Estimated $D_{app}$ for Pb diffusion in basalt and breccia.....	C-28
8.	Estimated $D_{eff}$ for Cs diffusion in basalt and breccia. ....	C-28

## **INTRODUCTION**

During the Cold War, the United States government conducted a series of nuclear weapons tests at various sites throughout the United States and its territories. The nuclear testing performed at these sites resulted in subsurface contamination from contaminants such as radionuclides (e.g., uranium,  $^{238}\text{U}$ , Pu, Am, and cesium,  $^{137}\text{Cs}$ ), organic compounds, toxic metals (such as lead, Pb), hydrocarbons, drilling mud and residues from plastics, epoxies, and drilling instrumentation (U.S. DOE, 1996). Because of their toxicity or radioactivity, many of these contaminants are considered to be health hazards (some, proven carcinogens) and consequently pose a threat to organisms that are exposed to them (including humans and wildlife). Thus, it is vitally important to assess the potential of these contaminants to reach the accessible environment where humans can ingest them—either by way of contaminated water supplies or through contaminated food chains.

Two factors primarily affect the transport and fate of contaminants in groundwater: (1) properties of the subsurface materials or the subsurface environment, and (2) physiochemical and biological properties of the contaminant (Knox et al., 1993). The degree to which contaminants interact with the soil matrix, therefore, will have a significant effect on the migration of such contaminants downstream. Conservative (nonreactive) ions and compounds, which are not affected by abiotic or biotic processes, essentially move with the velocity of the groundwater. Conversely, nonconservative (reactive) ions or compounds have the potential to be significantly retarded compared to groundwater flow if the proper conditions exist in the surrounding subsurface environment. Any attempt, therefore, to estimate the migration potential of contaminants requires that experimental studies be performed to evaluate the reactivity of these substances for the surrounding subsurface matrix through which the groundwater flows (Papelis, 1997).

The objective of this study was to estimate the rate of migration of reactive and nonreactive solutes (representative of inorganic contaminants found at underground nuclear test sites) through volcanic basalt and breccia from the Cannikin Test Site, Amchitka Island, Alaska. In an effort to predict the migration potential of these contaminants to reach surface waters (in particular the Bering Sea which lies approximately 1 mile away), batch equilibrium experiments were performed using Pb and Cs as reactive solutes and diffusion experiments were performed using bromide (Br) as a nonreactive solute. Lead and Cs were selected for the study because of their different reactive characteristics and because they may occur in the subsurface environment at the Cannikin site either as a result of their use in shielding of the nuclear device or as byproducts of the test performed at the site in November 1971. Bromide was chosen because of its nonreactive characteristics to allow a comparison regarding the movement of nonreactive and reactive solutes.

The remainder of this report is organized as follows. The characterization of each adsorbent, a brief discussion of the ions of interest (Pb, Cs, and Br) and the general experimental procedures are presented next. The results and discussion are presented subsequently, followed by a summary, conclusions and recommendations for further study.

## **MATERIALS AND METHODS**

### **Adsorbent Characterization**

Two adsorbents (hereafter referred to simply as sorbents) were used in this study: basalt and breccia. An extensive characterization was performed on each of these sorbents, which included mineralogy (solid structure), as determined by x-ray diffraction (XRD), soil pH measurement, major

and trace element analysis by x-ray fluorescence (XRF), solid morphology and composition as determined by scanning electron microscopy (SEM) and energy dispersive x-ray (EDX) spectroscopy, respectively, pore size distribution and specific surface area, as determined by nitrogen adsorption, porosity and density determination, and cation exchange capacity (CEC). This level of characterization is needed to define parameters that are important in the experimental design and that are required for the estimation of other geochemical transport parameters obtained from the experimental data.

A portion of each sorbent was first reduced in size, a step necessary for performance of small-scale batch equilibrium experiments. It should be noted that the sorption capacity of a solid is proportional to the total surface area available and the total surface area of nonporous particles is inversely proportional to the particle diameter. Thus, it is expected that higher sorption, per unit mass of sorbent, will occur as the particle size fraction is decreased. The size reduction and subsequent sieving resulted in nine size fractions, ranging in size from greater than 4 mm to less than 50  $\mu\text{m}$ . The 600 to 354  $\mu\text{m}$  size fraction was mainly used in the sorption experiments, although a comparison of sorption behavior was made using the 833 to 600  $\mu\text{m}$  size fraction as well.

### Sorbent Mineralogy

The mineralogy of the basalt and breccia was determined by XRD after particle size reduction. Spectra were collected in the 5 to 60° 2 $\theta$ -range using 0.03° 2 $\theta$  steps and Cu K $\alpha$  radiation ( $\lambda = 1.54060 \text{ \AA}$ ). Inspection of the spectra and an automated search of the peaks obtained is consistent with the presence of the following minerals for each sorbent: basalt–*major*: augite and laumontite; *minor*: analcime, augite, and magnesioferrite; breccia–*major*: plagioclase and chlorite; *minor*: laumontite, plagioclase, chlorite, and quartz. This composition agrees well with that given by Brown (1967) for basaltic rocks. All aforementioned minerals fall into one of the following major mineral groups: pyroxenes (augite), zeolites (laumontite, analcime), feldspars (plagioclase), chlorite, spinels (magnesioferrite), or quartz. A brief description of each of these mineral groups is provided below.

#### Pyroxenes

The pyroxene group is a broadly diverse mineral family whose various members constitute the most abundant and widespread of the ferromagnesian minerals in igneous rocks. In general, pyroxenes are defined as a group of dark, rock-forming silicate minerals, closely related in crystal form and composition with the general formula:  $A_2B_2[\text{Si}_4\text{O}_{12}]$ , where A = Ca, Na, Mg, or  $\text{Fe}^{2+}$ , and B = Mg,  $\text{Fe}^{2+}$ ,  $\text{Fe}^{3+}$ , Cr, Mn, or Al, with silicon sometimes replaced in part by aluminum (Jackson, 1997). Structurally, pyroxenes are all single-chain silicates (inosilicates) based on tetrahedral linkage. They are comprised of endless one-dimensional chains made up of  $\text{SiO}_4$  tetrahedra in which two apical oxygens are shared with adjacent tetrahedra. The individual chains are bound together by interstitial cations in roughly octahedral coordination (Blatt and Tracy, 1996). A structural subdivision divides the pyroxenes into clinopyroxenes, which crystallize in the monoclinic system and orthopyroxenes, which crystallize in the orthorhombic system. A detailed discussion on each of these subdivisions is not within the scope of this text and the reader is referred to Blatt and Tracy (1996), Jackson (1997), and Brown (1967) for further information. Augite, one of the minerals found in both the basalt and the breccia, falls into the clinopyroxene subgroup and is usually black, greenish black, or dark green.

## Zeolites

Zeolites are crystalline, hydrated aluminosilicates of alkali and alkaline earth cations that possess infinite, three-dimensional crystal structures (Ming and Mumpton, 1989). They are further characterized by their abilities to hydrate and dehydrate reversibly and to exchange some of their constituent cations, without major change of structure. As hydrous aluminosilicates, zeolites are analogous in composition to the feldspars, with Na, Ca, and K (rarely Ba or Sr) as their primary cations (Jackson, 1997). They are classified as tectosilicates, meaning they consist of three-dimensional frameworks of  $\text{SiO}_4^{4-}$  tetrahedra in which all oxygens of each tetrahedron are shared with adjacent tetrahedra. Such an arrangement reduces the overall Si:O ratio to 1:2, and if each tetrahedron were to contain Si as its central cation, the structure would be electrically neutral, as is quartz (Ming and Mumpton, 1989). In zeolite structures, however, some of the  $\text{Si}^{4+}$  is replaced by  $\text{Al}^{3+}$ , giving rise to a net negative charge within the framework, which is balanced by the incorporation of cations, in particular  $\text{Ca}^{2+}$ ,  $\text{Na}^+$ ,  $\text{K}^+$  or  $\text{Mg}^{2+}$ , in the cage structure. In general, zeolites are either white or colorless, though they have been tinted red or yellow due to impurities. Two zeolites, laumontite and analcime, were identified as either major or minor minerals in the sorbents used in this study. Laumontite is a white, monoclinic zeolite mineral having the formula:  $\text{Ca}[\text{Al}_2\text{Si}_4\text{O}_{12}] \cdot 4\text{H}_2\text{O}$ . This mineral can sometimes contain appreciable amounts of sodium and, on exposure to air, loses water, becomes opaque, and crumbles (Jackson, 1997). Analcime, the other identified zeolite, is a glassy, colorless to pink zeolite mineral with the general formula:  $\text{Na}[\text{AlSi}_2\text{O}_6] \cdot \text{H}_2\text{O}$ . It is a cubic zeolite, commonly found in diabase and alkali-rich basalts. For further information on these minerals, or on zeolites in general, the reader is referred to Ming and Mumpton (1989), Gottardi and Galli (1985), and Mumpton (1981).

## Feldspars

The feldspar group is unquestionably the most common mineral group in both the earth's crust and in igneous rocks. Feldspars are anhydrous tectosilicates of general formula:  $\text{M}[\text{Al}(\text{Al},\text{Si})_3\text{O}_8]$ , where  $\text{M} = \text{K}, \text{Na}, \text{Ca}, \text{Ba}, \text{Rb}, \text{Sr}, \text{or Fe}$  (Jackson, 1997). Structurally, the feldspars are framework aluminosilicates consisting of a three-dimensional continuous framework of tetrahedrally coordinated silicon and aluminum. All four corner oxygens in each  $\text{SiO}_4$  or  $\text{AlO}_4$  tetrahedron are linked to adjacent tetrahedra (Blatt and Tracy, 1996). Feldspars are usually white or nearly white in color and are clear and translucent, although they may sometimes be colored due to impurities. Plagioclase feldspars, one of the minor minerals identified in both the basalt and breccia, are simply those feldspars that are rich in Ca and/or Na, but with small amounts of K, as opposed to alkali feldspars (such as orthoclase), which are rich in K and Na, but have small amounts of Ca (Huang, 1989). For more information on feldspars, the reader is referred to Huang (1989) and Brown (1967).

## Chlorites

Chlorites are defined as a group of platy, monoclinic, usually greenish minerals having the general formula:  $(\text{R}_{+2},\text{R}_{+3})_6\text{AlSi}_2\text{O}_{10}(\text{OH})_8$ , where  $\text{R}_{+2} = \text{Mg}^{2+}, \text{Fe}^{2+}, \text{Mn}^{2+}, \text{or Ni}^{2+}$  and  $\text{R}_{+3} = \text{Al}^{3+}, \text{Fe}^{3+}, \text{Cr}^{3+}$  (Jackson, 1997; Barnhisel and Bertsch, 1989). There are four subgroups of this 2:1 layer clay mineral: trioctahedral chlorite (the most common chlorites), dioctahedral chlorite, di, trioctahedral chlorite, and tri, dioctahedral chlorite. Chlorites, being less stable than other clays when placed into acidic environments, have a high tendency to be altered. It is this tendency that accounts for significant amounts of  $\text{Mg}^{2+}$  and other cations that occupy exchange sites of clay minerals of such soils (Barnhisel and Bertsch, 1989). Chlorites in soil are largely inherited as primary minerals found in metamorphic or igneous rocks, or they occur as alteration products from minerals such as hornblende, biotite, and other ferromagnesium minerals. The structure of the most common

chlorite, trioctahedral chlorite, is composed of four sheets of polyhedra. Three of these sheets are chemically bound together to form a 2:1 layer that is structurally similar to mica, consisting of two tetrahedral sheets, one on each side of an octahedral sheet. The fourth sheet has been described in the literature in several ways, but is commonly expressed as an interlayer hydroxide sheet. Further discussion on this material is beyond the scope of this report and the reader is again referred to Barnhisel and Bertsch (1989) for additional information.

### Spinel and Quartz

The spinel group can be defined as a group of minerals of general formula:  $B_2[AO_4]$ , where A represents Mg,  $Fe^{2+}$  and  $Fe^{3+}$ , Zn, or Mn or any combination of these, and is in tetrahedral coordination by oxides, and B represents Al,  $Fe^{2+}$  and  $Fe^{3+}$ , or Cr and is in octahedral coordination by oxides (Jackson, 1997). Magnesioferrite, a major mineral found in the breccia, is defined as a black, strongly magnetic, cubic mineral of the spinel group having the formula:  $Fe_2^{3+}(Mg,Fe)^{2+}O_4$ .

Quartz is a crystalline, rock-forming mineral of the general formula  $SiO_2$ . This mineral is found in essentially all soils and parent materials and, next to feldspar, is the commonest mineral, occurring either in transparent hexagonal crystals (colorless, or colored by impurities) or in crystalline or cryptocrystalline masses (Jackson, 1997). A silicate mineral, quartz is classified as a tectosilicate comprised entirely of  $SiO_4$  tetrahedra in which each oxygen is linked to Si atoms of adjacent tetrahedra forming a three-dimensional framework structure.

### Major and Trace Element Analyses

To further quantify the mineralogical composition of the basalt and breccia samples, the XRD analysis was complemented by estimation of bulk elemental composition, as determined by x-ray fluorescence (XRF) and energy dispersive x-ray spectroscopy (EDX). The XRF results are shown in Tables 1a and 1b. The major element composition (Table 1a) is presented as weight percentage in terms of oxides. An average chemical composition of basalt according to LeMaitre (1976) is also shown for comparison purposes. Inspection of Table 1a shows that our analysis was in close agreement with that presented in the literature. Trace element composition for each sorbent is presented in Table 1b.

Table 1a. Major element composition of the breccia and basalt.

Major Element*	Breccia	Basalt	Basalt according to LeMaitre (1976)
$SiO_2$	49.5	50.5	50.06
$Al_2O_3$	16.4	16.1	15.94
$TiO_2$	1.13	1.07	1.87
$Fe_2O_3$	13.0	11.5	11.4
CaO	7.11	11.8	9.70
$K_2O$	1.74	1.95	1.08
$P_2O_5$	0.385	0.387	0.34
MnO	0.223	0.213	0.20
$Na_2O$	4.05	1.40	2.94
MgO	6.44	5.14	6.98

\* All data are given as percent weight and were normalized to account for losses on water molecules.

Table 1b. Trace element composition of the breccia and basalt.

Trace Element	Breccia (ppm)	Basalt (ppm)
Rb	24.30	19.46
Sr	290.10	473.15
Y	25.58	22.64
Zr	63.95	77.55
Nb	7.03	4.06
Cr	64.71	61.41

As shown in Table 1a, both sorbents have very similar compositions. Additionally, the table reveals that SiO<sub>2</sub> represents the majority of the sample by weight in both sorbents. This is somewhat expected because SiO<sub>2</sub> would be present as quartz or as a component of any aluminosilicate. Other components found to be present in substantial quantities include Al<sub>2</sub>O<sub>3</sub>, Fe<sub>2</sub>O<sub>3</sub>, CaO, Na<sub>2</sub>O, and MgO.

An examination of the bulk elemental composition using EDX was performed on the breccia sorbent only and the results were found to be very similar to those of the XRF analysis. Analysis of a general view of a breccia sample, shown in Figure 1 (Figures 1 through 6 are located at the end of this report), yielded the following component weight percentages: Na<sub>2</sub>O–3.82; MgO–3.61; Al<sub>2</sub>O<sub>3</sub>–17.99; SiO<sub>2</sub>–48.15; CaO–11.41; and Fe<sub>2</sub>O<sub>3</sub>–15.02.

### Particle Morphology

To obtain a better understanding of the morphology of the sorbents, each sample was examined by scanning electron microscopy (SEM). SEM is one of the most commonplace, powerful, and sophisticated techniques available for the examination of surface and near-surface characteristics of samples. In addition, an average composition of individual particles imaged with the SEM was determined using an energy dispersive x-ray (EDX) attachment to the SEM. A JEOL JSM-840A SEM/EDX was used to examine several areas of the sample under different magnifications.

An attempt was made to identify individual minerals in the sample by SEM/EDX. Analyses can be performed with a spatial depth resolution of about 1 to 2 μm and an accuracy of 5 to 10 percent (Papelis and Sloop, 1997). This allows a semi-quantitative identification of individual mineral crystals based on the relative abundance of common elements in minerals. It should be noted here, however, that because several different minerals may have similar composition in terms of oxides, independent information on the types of minerals present, for example from XRD, may be required for unambiguous mineral identification. The advantage of the technique, however, lies in the fact that individual mineral grains can be examined, as opposed to analysis by XRD, which yields an average bulk composition.

Thin-section examination of both sorbents identified several minerals as shown in Figures 1 through 5. Figures 2, 3, and 4 correspond to the basalt sample and identify the presence of plagioclase (feldspar), zeolites, spinels, and pyroxenes. This is consistent with the XRD analysis, which identified augite (a pyroxene), laumontite (a zeolite), plagioclase, and chlorite. Figures 5 and 6

correspond to the breccia sample and identify the presence of albite (a feldspar), plagioclase and orthoclase (feldspars), a zeolitic alteration product, pyroxene, and spinel. This, too, is consistent with the XRD analysis which identified analcime (a zeolite), augite, magnesioferrite (a spinel), laumontite, plagioclase, chlorite, and quartz. The advantage of the examination of thin sections is that the relative semiquantitative abundance of mineral groups can be determined.

### Bulk and True Density Analyses

The bulk and true densities of the sorbents were estimated by using the intact core samples and the following procedure. First, the sample was dried at 100 °C in an oven for 24 hours. The dry weight,  $w_d$ , of the sample was then measured and recorded. The total volume,  $V_T$ , of the dried sample was measured by placing the sample in a graduated cylinder and measuring the change in level of a surrounding medium. In this method, the surrounding medium consisted of quality glass spheres having a diameter between 425 and 300  $\mu\text{m}$ . This material was chosen so that a true measure of the total volume would be obtained rather than a skewed value, which might be obtained by using water (the dry sample might absorb water into the pore spaces, thereby yielding incorrect results). The size fraction chosen for the glass spheres allowed for an acceptable degree of compaction, yet prevented spheres from migrating into the pore spaces. Once the volume of the dry sample was determined, the bulk density ( $\rho_b$ ) could be obtained using Equation (1):

$$\rho_b = \frac{\text{mass dry sample}}{\text{total volume dry sample}} = \frac{w_d}{V_T} \quad (1)$$

The sample was then immersed in NANOpure™ water (high purity water with at least 18M $\Omega$  cm resistivity) and placed in a sealed vacuum chamber at ambient temperature to achieve saturation. Once saturated, the surfaces were wiped off and the saturated weight determined. Assuming the water density is 1.00 g/cm<sup>3</sup> at 25 °C (approximate water temperature) the total pore volume,  $V_p$ , of the rock was then determined as the difference between the dry and saturated sample weights divided by the density of the water. The true density was then determined as the dry weight divided by the volume of the solid ( $V_T - V_p = V_{\text{solid}}$ ). Total porosity,  $\epsilon$ , is the ratio of total pore volume to total sample volume and can therefore be determined by the following equation:

$$\epsilon = \frac{V_p}{V_T} \quad (2)$$

The average bulk density measured for the basalt sample was 2.21 g/cm<sup>3</sup> and the average true density was 2.51 g/cm<sup>3</sup>. The bulk and true densities for the breccia sample were 2.13 g/cm<sup>3</sup> and 2.46 g/cm<sup>3</sup>, respectively. Likewise, it was determined that the porosity of the basalt sample was approximately 11 percent and that of the breccia was approximately 13 percent. These values are consistent with those reported by Freeze and Cherry (1979), who list an average porosity value of brecciated basalts as 10 percent and by Fetter (1994), who states that basalts generally have a porosity between 1 and 12 percent.

### Specific Surface Area and Pore Size Distribution

The specific surface area and the pore size distribution of the sorbents were determined based on nitrogen adsorption measurements, using a Gemini 2370 Analyzer and the BET model (Brunauer et al., 1938). This method can be used to obtain an estimate of the specific surface area of sorbents having surface areas from 1 to several hundred m<sup>2</sup>/g (using nitrogen adsorption). Although the

method has several shortcomings, it continues to be the most widely used and general method for particle surface area estimation (Gregg and Sing, 1982). The measured specific surface areas for the two size fractions used for the sorption experiments are shown in Table 2.

The specific surface area of nonporous particles is inversely proportional to particle size, i.e., as the particle size increases, the specific surface area decreases. Inspection of Table 2 does indeed reveal a small dependence of specific surface area on particle dimensions for both sorbents. One should note, however, the relatively small change in surface area between the larger and smaller size fractions for the basalt material. Such behavior can most likely be attributed to the fact that the majority of the surface area is internal, in which case one would not expect to see much difference in specific surface area with size. The presence of zeolites, as determined by XRD analysis, is consistent with these findings because zeolites possess an internal cage-like framework structure giving them a large internal surface area. The small variations of surface area between particle sizes can most likely be attributed to decreased accessibility of internal pores with increasing particle size.

Table 2. Measured specific surface areas of basalt and breccia sorbents.

Sorbent	Size Fraction (mm)	Surface Area (m <sup>2</sup> /g)
Basalt	833-600	2.4024
	600-354	2.537
Breccia	833-600	8.3936
	600-354	9.432

Inspection of the table also reveals the differences in surface areas between the two sorbent types with that of the breccia being almost four times larger than that of the basalt. It is important to be aware of this because it enables normalization of solute sorption data to surface area and, ultimately, allows a meaningful comparison to be made regarding sorption of ions as a function of sorbent type. For example, the breccia would require roughly ¼ the solid concentration of the basalt to have roughly the same overall surface area.

The results of pore size analysis can be seen in Table 3. (Note: The results presented are for the 600-354 µm size fraction and are averaged values of duplicate analyses). As can be seen from the table, the average pore diameter (4V/A) is 205.18Å for the basalt, and 153.43Å for the breccia. Based on the average pore size diameter, these materials can be classified as mesoporous, referring to materials with pore size diameters between 20 and 500Å. Figures 7 and 8 illustrate the adsorption and desorption branches of the nitrogen isotherms for the basalt and the breccia, respectively.

Table 3. Pore size measurements for the basalt and breccia.

	Basalt	Breccia
BJH Adsorption Average Pore Diameter (4V/A)	240.48Å	158.75Å
BJH Desorption Average Pore Diameter (4V/A)	122.52Å	90.42Å
Average Pore Diameter (4V/A)	205.18Å	153.43Å

Inspection of both figures shows the results of each duplicate experiment to be in close agreement with each other. Table 3 shows the average pore diameters (4V/A) calculated from the

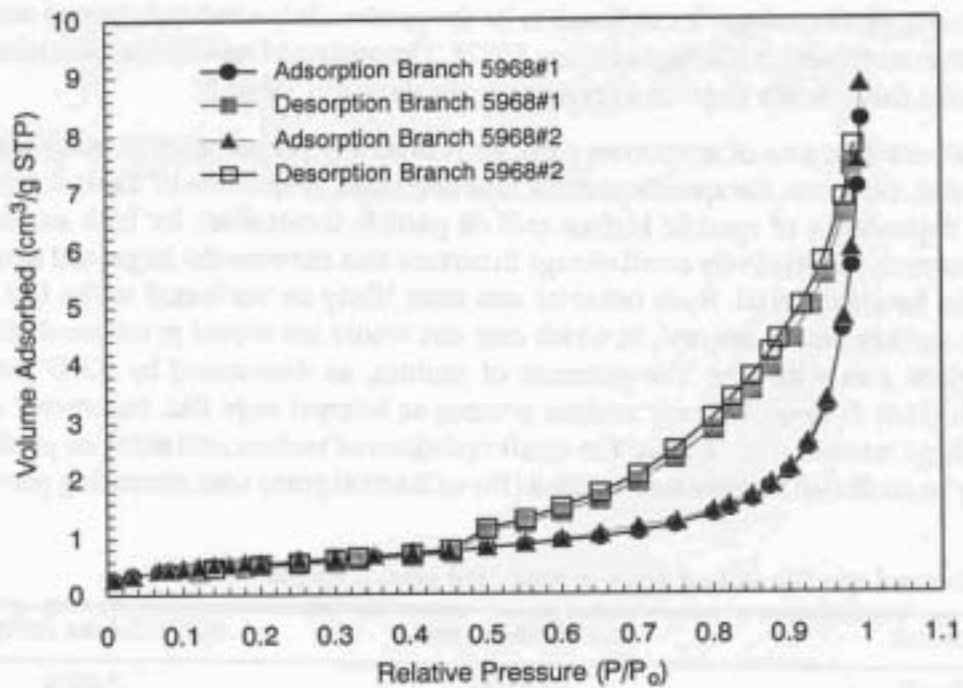


Figure 7. Isotherm of nitrogen adsorption/desorption on the basalt.

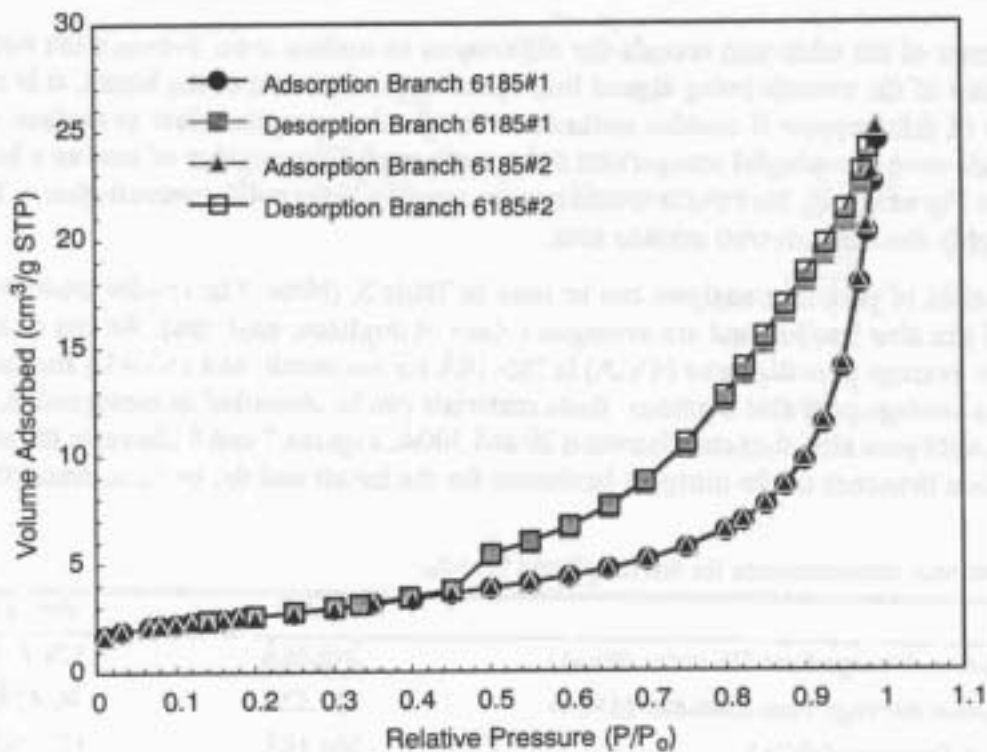


Figure 8. Isotherm of nitrogen adsorption/desorption on the breccia.

adsorption and desorption branches of each sorbent. The average pore diameter estimated from the adsorption branch (as averaged from duplicate analysis) was 240.48Å and 158.75Å for the basalt and the breccia, respectively. The average pore diameter estimated from the desorption branch was 122.52Å and 90.42Å for the basalt and breccia, respectively.

In conclusion, it can be seen that the basalt has a somewhat larger average pore diameter than the breccia. This is consistent with the finding that the breccia has the higher specific surface area because, as previously mentioned, specific surface area is inversely proportional to size; thus the smaller pore sizes are expected to have larger surface areas.

#### Soil Solution pH and Cation Exchange Capacity

The soil solution pH was measured by suspending an amount of the sorbent in NANOpure™ water and allowing it to equilibrate for approximately 24 hours. The pH values obtained for solid concentration of 1 g/L were 8.511 and 8.765 for the basalt and breccia, respectively. These results become important, as is discussed later in this report, when looking at the sorption of Pb on the sorbents. It is at a pH of approximately 8 that Pb sorption on each sorbent most closely resembles a linear isotherm.

The cation exchange capacity (CEC) was determined according to Busenberg and Clemency (1973). The measurements for each sorbent were performed in duplicate and the final value obtained was an average of the two individual experiments. The CEC of the basalt was 86.3 meq/kg, and the CEC of the breccia was 183 meq/kg. Note that the CEC of the breccia was approximately twice that of the basalt. This can most likely be attributed to the fact that the breccia has a higher surface area than the basalt, and potentially greater number of reactive sites for exchanging ionic species per unit mass of material. Thus, it is no surprise that the material with the higher surface area has the higher CEC.

#### **The Elements of Interest**

##### Lead

Lead is perhaps the most common of the toxic heavy metal elements and is normally found in sulfides forming the common mineral galena, PbS. The element occurs naturally in the earth's crust with an average concentration of 14 parts per million (ppm). In soils, concentrations can range from 2-200 parts per billion (ppb) for normal, unpolluted soils to as high as 1-30 ppm in polluted soils (Cox, 1995).

Lead is introduced naturally into the environment from the erosion of lead-containing rocks and through gaseous emissions during volcanic activity. In addition to natural emissions, anthropogenic sources of lead include lead smelting and refining, automobile emissions, lead-acid storage batteries, the production of alkyllead compounds for use as anti-knock agents in gasoline, roofing materials, pigments (white lead,  $Pb_3(CO_3)_2(OH)_2$ ), pipes for domestic water systems, manufacturing of cable sheathings, sheet, pipe, foil and tubes, solders and alloys, ammunition, the production of various inorganic compounds, and protective shields for nuclear chemists, x-ray operators, and radiologists (Waldron, 1980; Cox, 1995).

Lead primarily affects the blood, the nervous system, and the kidney and symptoms of lead poisoning include anemia, anorexia, and abdominal pains, as well as neurological effects such as irritability, mood disturbance, and loss of coordination. The residence time of lead in the body is very long, one reason being that a significant amount is taken up in the bones where the  $Pb^{2+}$  replaces some  $Ca^{2+}$  in calcium phosphates (Cox, 1995).

## Cesium

A rare Group IA element, Cs has little use, no known biological role, and is non-toxic. Chemically, cesium resembles rubidium and potassium, and is characterized as being a silvery-white, very soft metal which reacts rapidly with oxygen and explosively with water. Cesium occurs as the hydrated aluminosilicate pollucite,  $Cs_4Al_4Si_9O_{26} \cdot H_2O$ , but the world's only commercial source is at Bernic Lake, Manitoba, and Cs is mainly obtained as a byproduct of the lithium industry (Greenwood and Earnshaw, 1984; Emsley, 1989). It is not very abundant in the Earth's crust, there being only 7 ppm present. Detectable amounts are found in plant and animal organisms, mineral waters, and soils (Hart, et al., 1975).

Cesium metal is used in photoelectric cells, spectrographic instruments, scintillation counters, radio tubes, military infrared signaling lamps, and various optical and detecting devices. Cesium compounds are used in glass and ceramic production, as absorbents in carbon dioxide purification plants, as components of getters in radio tubes, and in microchemistry. Cesium salts have been used medicinally as antishock agents after administration of arsenic drugs (Hart, et al., 1975).

Although Cs is not known to be toxic, radioactive isotopes of cesium formed as fission products from uranium are indeed of environmental concern. Cesium-137 is a significant health hazard because its long half life of about 30 years allows it to persist in the environment as a highly radioactive element. Besides its persistence and high activity,  $^{137}Cs$  has the further insidious property of being mistaken for potassium by living organisms and taken up as part of the fluid electrolytes, thereby becoming bioaccumulated through the food chain (Hammond, 1992). One positive function of the radioactive isotope, however, is its use in the treatment of cancer.

## Bromine

Bromine is a rather rare element in the earth's crust and occurs exclusively as the bromide ion,  $Br^-$ . Being chemically similar to chlorine, it exhibits many of the same characteristics, such as being very soluble and relatively abundant in the ocean. Most bromine used for industrial purposes is extracted from the sea water or other natural brines. In most cases, the element is not used in its elemental or ionic form, but is converted to organic bromine compounds such as ethylene dibromide,  $CH_2BrCH_2Br$ , which is used as a fuel additive. Other organic bromides are used as pesticides or as fire retardants for synthetic fibers (Cox, 1995).

As the bromide ion, the element is universally present in life along with the similar chloride. It is not thought to be an essential element, though several bromide compounds have been found in marine organisms. Like chlorine, the elemental form  $Br_2$  is highly toxic. Likewise, elevated concentrations of  $Br^-$  appear to have a depressive effect on the nervous system contributing to its use as a sedative and as an anti-convulsant for treating epilepsy.

## **Experimental Procedures**

### Batch Equilibrium Sorption Experiments with the Cannikin Site Core Samples

Batch equilibrium sorption experiments, using the reactive Pb and Cs solutes only, were conducted in individual 12-mL polypropylene centrifuge tubes. A specific amount of solid was added to the centrifuge tubes, the amount depending on the final solid concentration desired. Almost all experiments were performed using 1 g/L solid. A variable amount of either 0.1 M  $HNO_3$  (nitric acid) or 0.1 M NaOH (sodium hydroxide) was added to adjust the pH to the approximate final pH value desired. The amounts of acid and base required for pH adjustment were determined by trial

and error. Typically, a pH range between 5 and 9 was targeted. After the initial acid or base addition, the solution was allowed to equilibrate without further pH adjustments.

A set of nine individual centrifuge tube-reactors was set up at a time with varying target pH values. The first of these was a control tube to which no soil was added. Approximately 59  $\mu\text{L}$  of either  $1.7 \times 10^{-5}$ ,  $1.7 \times 10^{-4}$ ,  $1.7 \times 10^{-3}$ , or  $1.7 \times 10^{-2}$  M metal ion were added to the centrifuge tubes to achieve the desired final total metal concentration in the samples, ranging from  $10^{-7}$  to  $10^{-4}$  M. The adsorbate added was either  $\text{Pb}(\text{NO}_3)_2$  (lead nitrate) or  $\text{CsNO}_3$  (cesium nitrate) depending on the experiment being performed. The necessary quantity of NANOpure™ water was added to result in a final solution volume of 10 mL. All reagents used were of ACS grade quality grade or better. NANOpure™ water was used exclusively for all solutions prepared.

The individual centrifuge tubes were allowed to equilibrate for at least 24-hours by end-over-end rotation at 8 rpm. Preliminary experimental work showed that this equilibration time was indeed adequate. Although true equilibrium, in a strict thermodynamic sense, was most likely not reached within the 24 hour equilibration period, the conclusions presented here are still valid, based on the much shorter time scale for the sorption processes described here, compared to processes such as solid solution formation and phase transformations, which would tend to shift the position of equilibrium.

Upon reaching equilibrium, the final pH of the suspension was measured using an Orion model 720 pH meter with an Orion Ross glass combination electrode. The pH meter was calibrated daily before use with pH 4.00, 7.00, and 10.00 buffers. Immediately following the pH measurement, solid-solution separation was achieved using a Marathon K/R 21 centrifuge and centrifuging the samples at 9000 rpm for 30 minutes. After centrifugation, a 2-mL aliquot was removed from the supernatant and acidified with 24  $\mu\text{L}$  of concentrated high purity  $\text{HNO}_3$  before analysis.

Ion concentrations of the aliquots were measured using a Perkin-Elmer 4110 ZL atomic absorption spectrophotometer equipped with a graphite furnace and Zeeman background correction. The relative fractional uptake (percent sorbed) of the ions by the sorbent was determined by comparing the ion concentrations in the supernatant to the concentration of the control sample. The equation used to determine the percent sorbed is given by:

$$\% \text{ Sorbed} = \frac{(C_o - C_{eq})}{C_o} \times 100 \quad (3)$$

where:  $C_o$  = total concentration of metal added to sample (mol/L); and  $C_{eq}$  = equilibrium concentration of metal remaining in the supernatant (mol/L)

Most experiments were conducted in synthetic groundwater having a composition representative of that found in the field. This choice was made because use of partitioning coefficients to predict the fate and transport of inorganic contaminants in natural hydrogeological environments requires estimation of the coefficients under identical geochemical conditions to those found at the site being studied. Failure to do so may result in severe over- or underestimation of contaminant transport. An analysis of both, the site and synthetic groundwater can be found in Table 4.

Table 4. Composition of site and synthetic groundwater.

Species	Site Groundwater (mg/L)	Site Groundwater (mol/L)	Synthetic Groundwater (mol/L)
SiO <sub>2</sub>	3.1-3.4	5.66E-04-	-
Al <sup>3+</sup>	-	-	-
Fe <sup>3+</sup>	<0.01	-	-
Mn <sup>2+</sup>	0.75-3.5	6.19E-05	-
Mg <sup>2+</sup>	<0.1-170	6.99E-03	6.99E-03
Ca <sup>2+</sup>	260-1900	4.74E-02	4.74E-02
Sr <sup>2+</sup>	2.2-21	2.28E-04	-
Li <sup>+</sup>	0.2-0.5	7.20E-05	-
Na <sup>+</sup>	1980-8700	3.65E-01	3.65E-01
K <sup>+</sup>	20-120	3.07E-03	3.07E-03
HCO <sub>3</sub> <sup>-</sup>	0-400	7.05E-04	7.05E-04
CO <sub>3</sub> <sup>2-</sup>	0	0.00E+00	0.00E+00
SO <sub>4</sub> <sup>2-</sup>	890-2000	1.87E-02	1.87E-02
Cl <sup>-</sup>	3000-16000	4.51E-01	4.39E-01
F <sup>-</sup>	<0.1-1.0	-	-
NO <sub>3</sub> <sup>-</sup>	<0.1-1.0	3.23E-06	-
PO <sub>4</sub> <sup>3-</sup>	<0.1-5.4	-	-
Note: pH		6.9	~7.8

### Diffusion Experiments with the Cannikin Site Core Samples

Diffusion experiments were conducted using small cores. The core (having typical dimensions no larger than 1½" x ¾" x ¾") was cut from the full core sample using a water mill saw and the bulk density, true density, and porosity determined as described in the previous section. Once the bulk density, true density, and porosity of the sample were determined, the diffusion experiments were conducted as follows.

The core was first saturated in a 0.1M solution of sodium bromide (NaBr) prepared using the synthetic groundwater. The saturation process was continued until no change in mass occurred. On average, saturation required approximately three weeks.

Prior to beginning the diffusion experiments, all but one outer surface of the sample were sealed with Varathane, a clear floor finish, to ensure that the bromide tracer was only able to diffuse out through the exposed end of the core. The experimental apparatus in which the diffusion experiments were conducted is shown in Figure 9. Each apparatus consisted of a one-liter mason jar having a tight-fitting screw-type lid. Each lid was equipped with a rubber septum for sampling and a threaded rod to which the core sample was attached and suspended above the underlying solution. The threaded rod allowed the height of the core sample to be adjusted to maintain constant contact with the underlying reservoir of solution. When using the bromide tracer, this underlying solution was 500 mL of NANOpure water. Each cell was also fitted with a 6-in long, 18-gauge

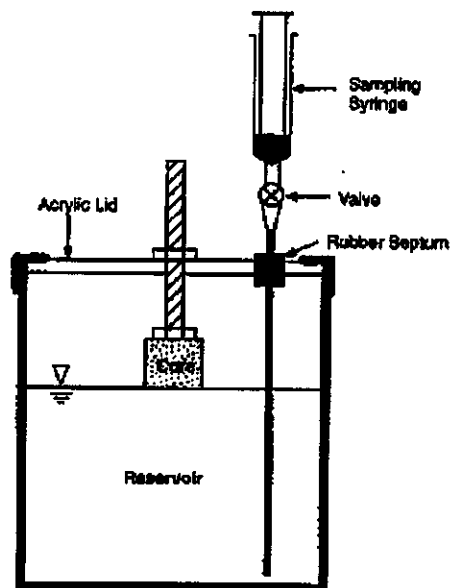


Figure 9. Experimental apparatus used in the diffusion experiments with NaBr.

needle, permanently placed through the rubber septum. This allowed for the collection of 2-mL samples of reservoir solution. The collected samples were then analyzed using an Orion 94-35 bromide selective electrode and an Orion 90-02 double junction reference electrode to determine the relative change in Br concentrations with time. As a check, some samples were additionally analyzed by ion chromatography (IC) to test the accuracy of the ion selective electrode.

## RESULTS AND DISCUSSION

The discussion of the results is divided into three sections. The first section presents a discussion of the results of the batch equilibrium sorption experiments for both the basalt and the breccia. This section is further subdivided into three parts: (1) lead sorption, (2) cesium sorption, and (3) isotherm parameter estimation. The second section presents the results of the diffusion experiments for both sorbents, followed by a discussion of the calculated diffusion parameters. Finally, the third section presents a comparison of the data for each sorbent where any similarities or differences are identified and discussed.

### Sorption of Pb and Cs on Cannikin Basalt and Breccia

#### Lead Sorption

Sorption of Pb on 1.0 g/L basalt at concentrations ranging from  $10^{-4}$  to  $10^{-6}$  M in synthetic groundwater (ionic strength  $\approx 0.5$  M) is shown in Figure 10. Inspection of this figure shows that, in general, the fractional uptake is a function of Pb concentration, decreasing with increasing metal concentration. For example, sorption of  $10^{-4}$  M Pb ranges from approximately 1 percent at a pH around 4 to 95 percent at a pH around 10. Sorption of  $10^{-6}$  M Pb at these same pH values is somewhat higher, approximately 18 percent at a pH around 4 to 96 percent at a pH around 10. One should note that, although the fractional uptake decreases with increasing concentration (as a *fraction* of total metal concentration sorbed), the total metal sorbed is actually increasing. The behavior of Pb displayed in these graphs is typical for a cation sorbing on amphoteric sites, i.e., increasing sorption

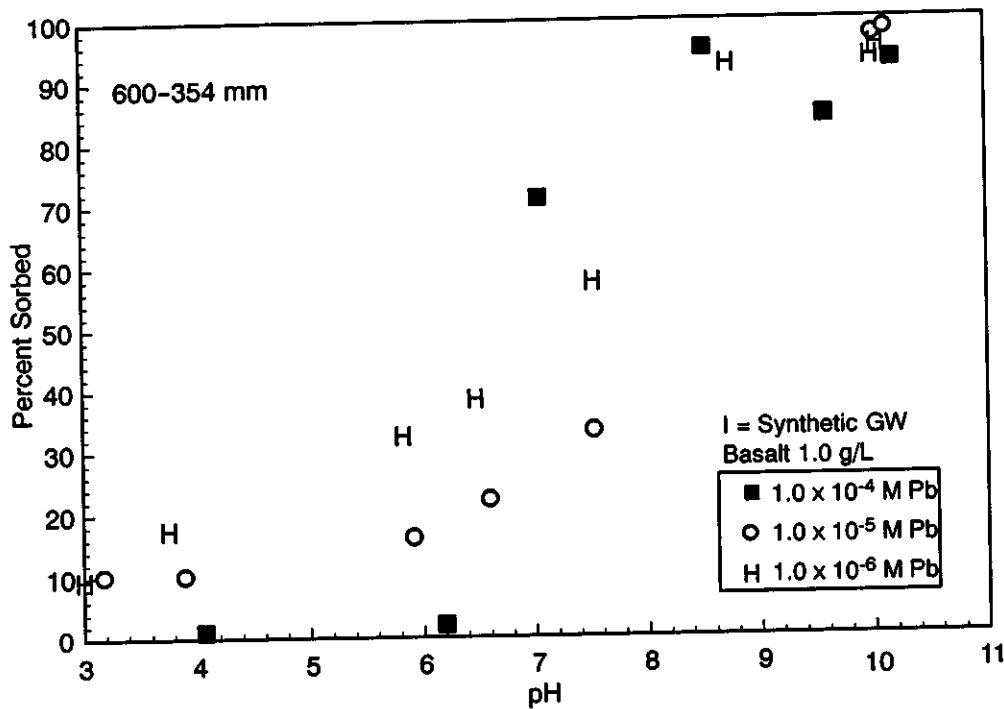


Figure 10. Sorption of Pb on 1.0 g/L basalt.

with increasing pH. For example, inspection of Pb sorption at  $10^{-5}$  M Pb clearly shows the fractional uptake of Pb increasing from approximately 10 percent at a low pH of 3 to a fractional uptake of essentially 99 percent at a pH of approximately 10. This pH-dependent sorption behavior suggests that the  $Pb^{2+}$  sorption is limited to amphoteric sites. Internal, permanent charge, cation-exchange sites are apparently inaccessible at a high ionic strength such as that used in this experiment. Formation of pH-dependent surface precipitates is also possible. Consideration of the sorption of  $10^{-4}$  M Pb reveals a sharp increase in the percent Pb sorbed between pH of 6 and 7. Such an abrupt increase in slope is a good indication that Pb surface or bulk precipitates may be forming. Unfortunately, however, macroscopic studies alone cannot be used to distinguish between different types of sorption mechanisms. Additional spectroscopic experiments would be required to identify the mechanism as absorption, adsorption, or surface precipitation and, specifically, whether the ion is binding as an inner- or outer-sphere complex. The fact that Pb shows considerable sorption at such a high ionic strength is indicative that it is most likely forming a strong, inner-sphere complex. For more information regarding these binding mechanisms, see Papeis (1996).

Sorption of Pb on 1.0 g/L breccia at concentrations ranging from  $10^{-4}$  to  $10^{-6}$  M and using synthetic groundwater (ionic strength  $\approx 0.5$  M) is shown in Figure 11. Inspection of this figure shows a sorption pattern similar to that of Pb sorption on the basalt, i.e., decreasing fractional uptake with increasing metal concentration. Likewise, we see that sorption of Pb on the breccia follows a similar pH-dependent behavior with percent Pb sorbed increasing from approximately 2 percent at pH 3 to 98 percent at pH 10 for the  $10^{-5}$  M Pb concentration. This pH-dependent sorption behavior, again, suggests that the internal cation-exchange sites are not accessible at the high ionic strength of the synthetic groundwater. Thus, Pb sorption on the breccia appears to be the result of sorption on external, pH-dependent surface sites.

For comparison purposes, a plot was made showing the difference in sorption behavior of Pb between the basalt and the breccia. Inspection of Figure 12 shows, in general, higher sorption on the

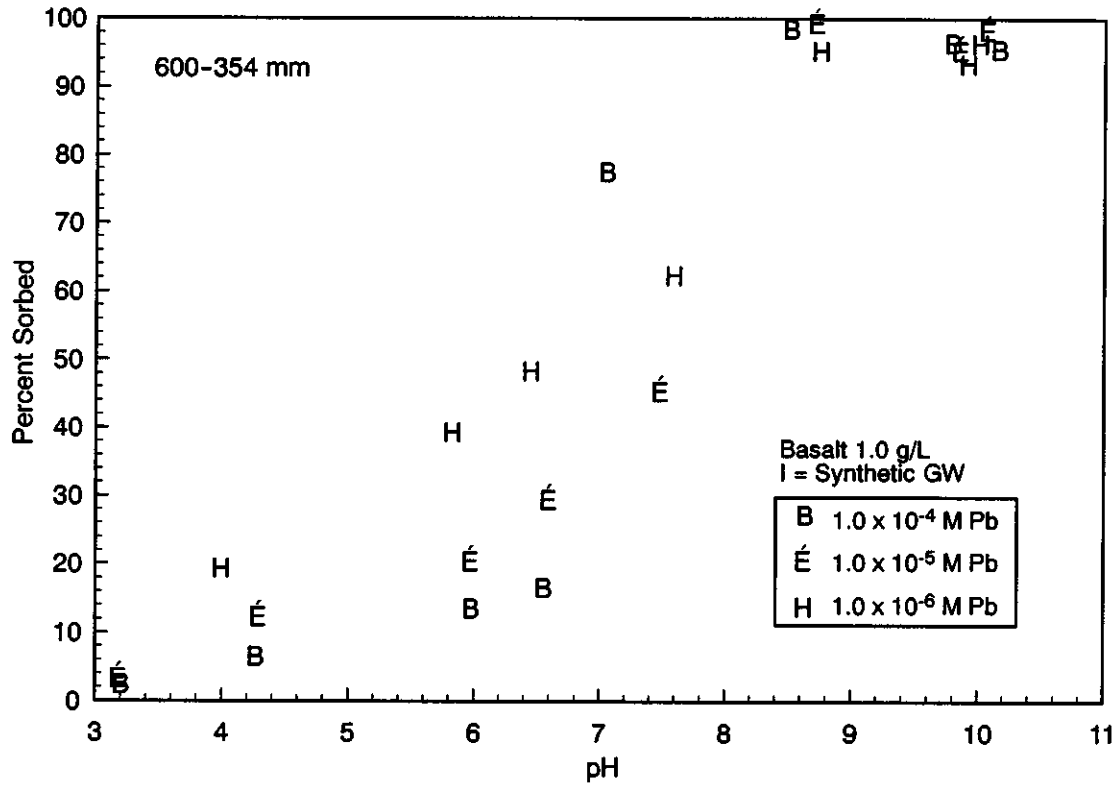


Figure 11. Sorption of Pb on 1.0 g/L breccia.

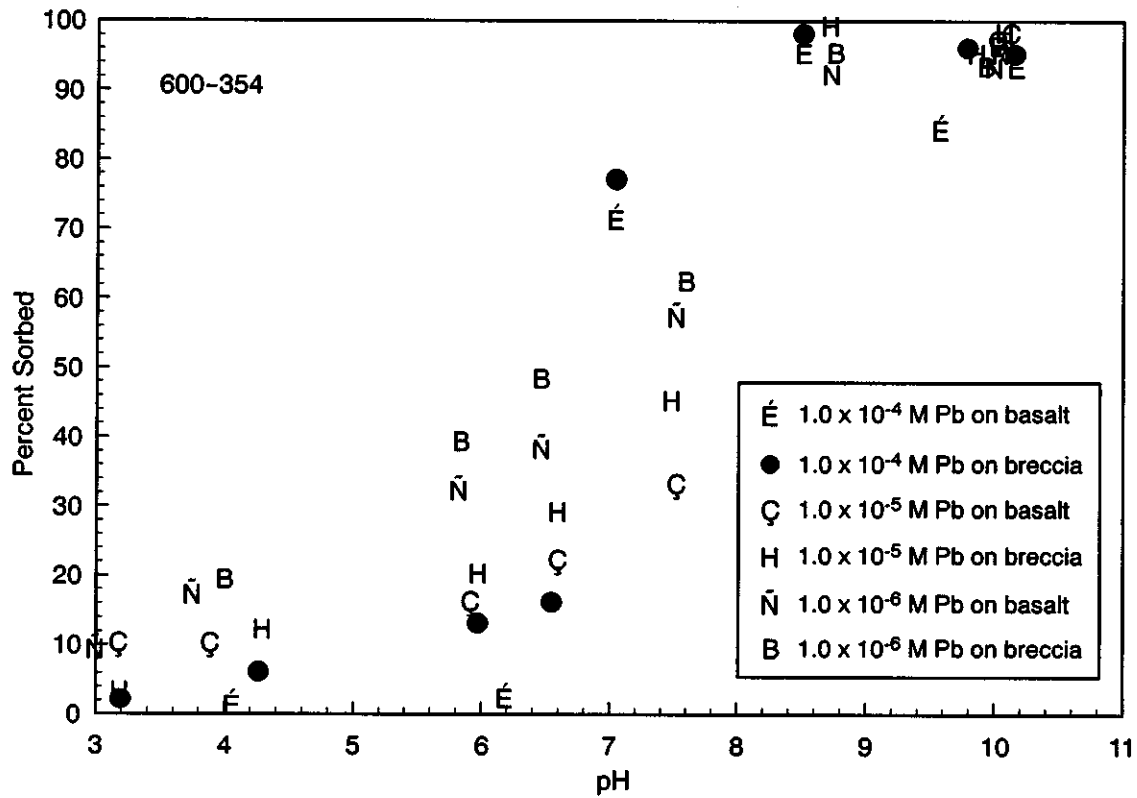


Figure 12. Sorption of  $10^{-4}$  to  $10^{-6}$  M Pb on basalt and breccia.

breccia at all concentrations. This is expected because the breccia, having approximately four times the surface area of the basalt, would have a higher number of sorption sites available to which ions could bind.

To obtain an understanding of how the extent of metal sorption on each sorbent varied with particle size, experiments were performed using Pb and a slightly larger size fraction, i.e., 833 to 600  $\mu\text{m}$ . The results of these experiments, using concentrations ranging from  $10^{-4}$  to  $10^{-6}$  M Pb can be seen in Figures 13 and 14 for the basalt and breccia, respectively. Inspection of these figures does show a slight increase in sorption as particle size decreases, which is expected as the smaller size fractions generally have a larger surface area. Because these size fractions are not very different, however, the difference in sorption is not significantly pronounced. Information regarding how the extent of sorption varies as a function of particle size is important because, at the actual field site, various types and scales of assemblages are present. Typically, as the scale increases, the reactivity of these assemblages decreases and it is thus important to keep this in mind when modeling solute transport.

### Cesium Sorption

Unlike Pb sorption, Cs sorption on the basalt was essentially nonexistent when using the synthetic groundwater. This behavior indicates that, not only was Cs unable to compete effectively with other cations for internal cation exchange sites, but it was unable to bind to the amphoteric surface sites as well. Such behavior is somewhat expected because Cs is not readily hydrolyzable as is the  $\text{Pb}^{2+}$  cation and is thus not prone to making strong binding complexes with pH-dependent surface sites. To test this hypothesis, the sorption behavior of Cs was also investigated using a 0.01M  $\text{NaNO}_3$  (sodium nitrate) background electrolyte concentration. Figure 15 shows the fractional uptake of  $1 \times 10^{-6}$  M Cs on 1.0 g/L of basalt and breccia in 0.01M  $\text{NaNO}_3$ . It can be seen from this figure that Cs is able to sorb and that fractional uptake is weakly influenced by pH except at extremely low pH. At such low pH values Cs is in competition with the  $\text{H}^+$  ion, which is present in concentrations 2-3 orders of magnitude higher. In general, the behavior displayed suggests that sorption of Cs by both sorbents is primarily controlled by sorption on cation exchange sites. The dependence of Cs sorption on ionic strength is a good indication that it is forming outer-sphere sorption complexes, as expected for an alkali metal. Note, also, the slightly higher sorption occurring on the breccia which, again, results from it having the higher specific surface area.

### Isotherm Parameter Estimation

The fractional uptake data obtained from the batch sorption experiments with Pb and Cs were used to construct sorption isotherms and to determine equilibrium partitioning coefficients. The amount of solute sorbed onto the soil can be calculated as the difference in mass of the solute in solution before and after reaction. As a result of the batch equilibrium experiments, it is possible to plot the mass sorbed per unit mass of soil,  $S$ , as a function of the equilibrium concentration of solute remaining in solution,  $C_{\text{eq}}$  (Fetter, 1994). This graphical representation is known as a *sorption isotherm*.

Several sorption isotherms have been developed and used over the years, however, the most commonly used are the linear, Freundlich, and Langmuir isotherms (Papelis, 1997). Because only the linear and Freundlich models were used in this study, they are discussed below. For more information on the Langmuir model, the reader is referred to Stumm and Morgan (1996), Drever (1997), Ruthven (1984), and Morel and Hering (1993).

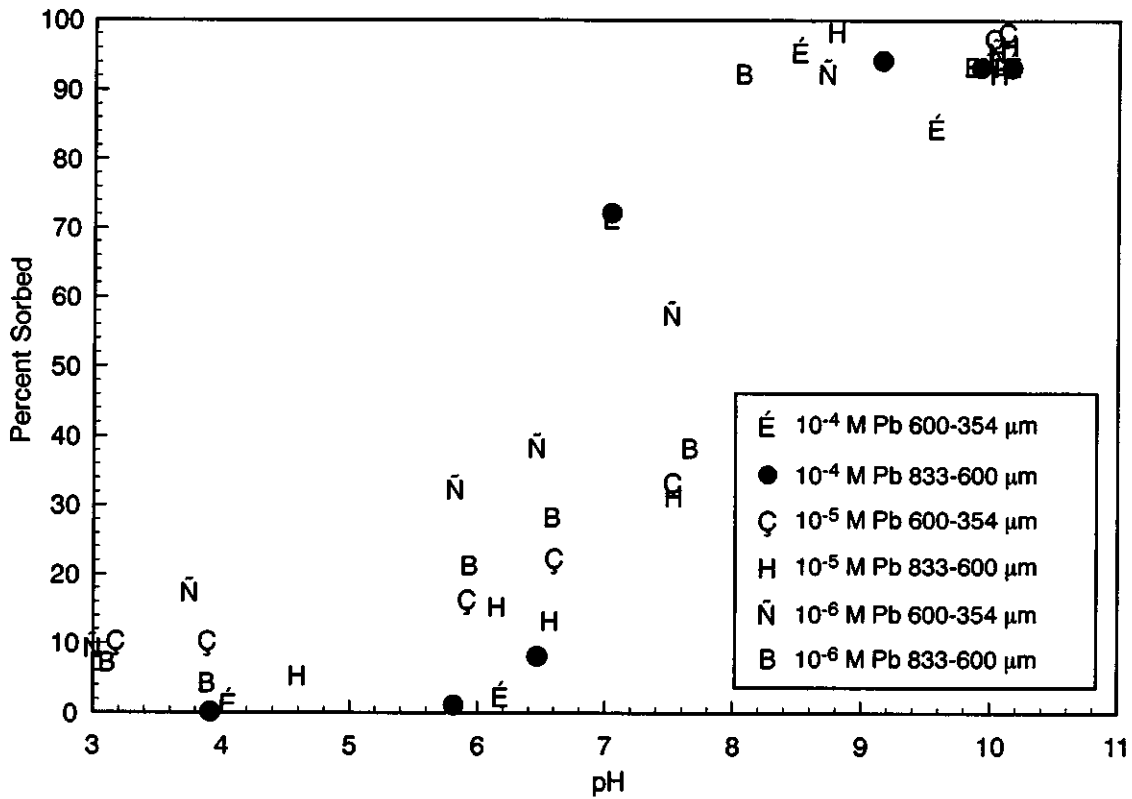


Figure 13. Comparison of sorption of 10<sup>-4</sup> to 10<sup>-6</sup> M Pb on larger and smaller size fractions of basalt.

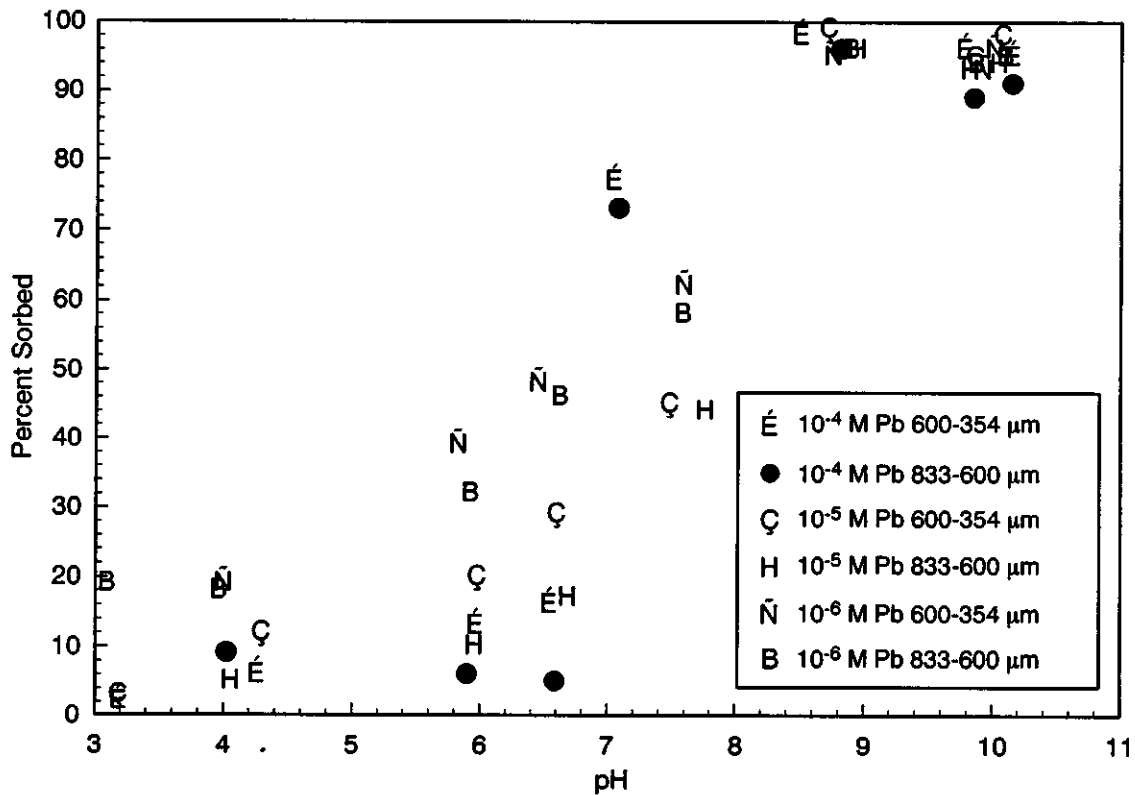


Figure 14. Comparison of sorption of 10<sup>-4</sup> to 10<sup>-6</sup> M Pb on larger and smaller sizes fractions of breccia.

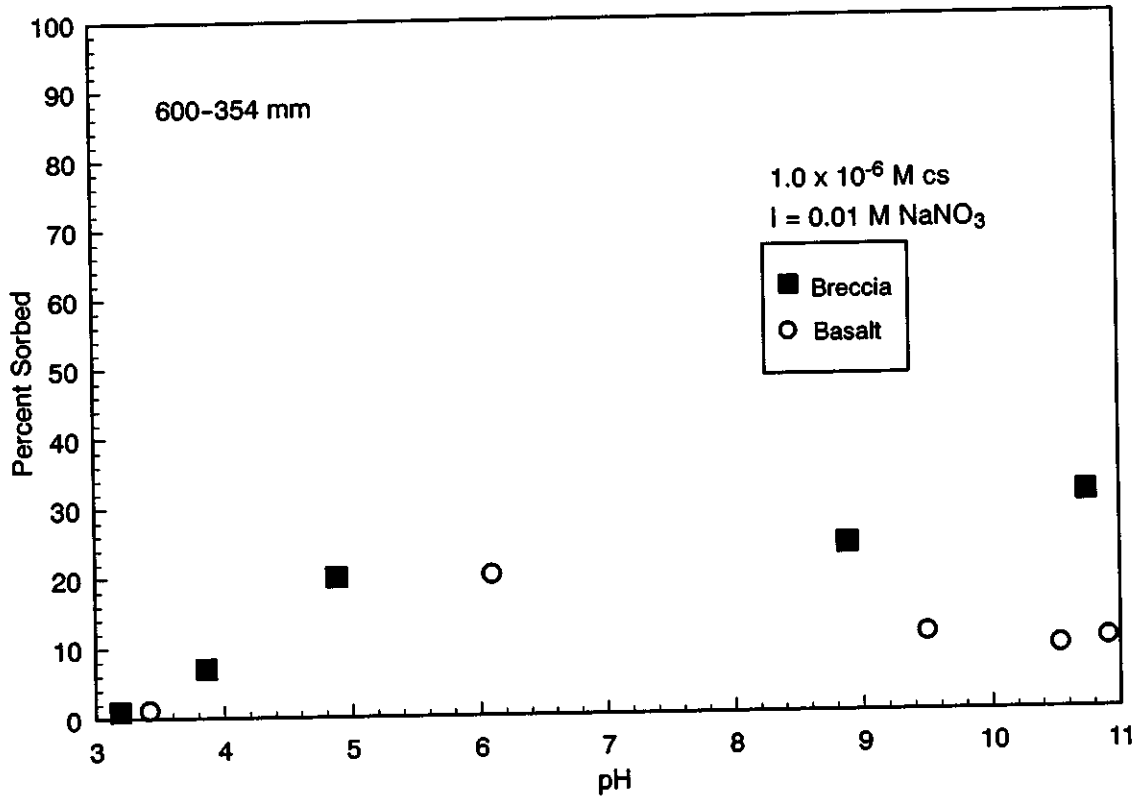


Figure 15. Sorption of  $1 \times 10^{-6}$  M Cs on 1.0 g/L basalt and breccia.

The linear isotherm assumes that the amount of contaminant sorbed by the soil matrix is directly proportional to the concentration of the compound in solution (Travis and Etnier, 1981). The equation describing the linear isotherm is given as:

$$S = K_d C_{eq} \quad (4)$$

where  $S$  = amount of solute sorbed (mol/kg solid),  $C_{eq}$  = concentration of solute in solution (mol/L), and  $K_d$  = distribution coefficient (L/kg).

In most instances, the  $K_d$  value is the sought-after parameter and is used in various transport codes to model the migration of hazardous ions in the subsurface environment. The numerical value of the distribution coefficient is a function of the properties of the solid and the composition of the solution and thus cannot be easily transferred from one system to another. Furthermore, use of the  $K_d$  assumes that the isotherm is truly linear and that the affinity of the sorbate for the sorbent remains the same for all levels of  $C_{eq}$ . Utilization of such a parameter when the above assumptions are not true may result in gross errors in sorption behavior predictions.

When sorption data do not exhibit a linear relationship, the Freundlich isotherm is often used instead. The Freundlich isotherm is the oldest of the nonlinear sorption isotherms and has been widely used to describe the sorption of solutes by soils (Travis and Etnier, 1981). The Freundlich isotherm is given as:

$$S = K_f C_{eq}^{1/n} \quad (5)$$

where  $S$  = amount of solute sorbed (mol/kg solid),  $C_{eq}$  = concentration of solute in solution (mol/L),  $K_f$  = the Freundlich constant ((mol/kg)/((mol/L)<sup>1/n</sup>)), and  $1/n$  = the measure of nonlinearity (dimensionless).

The parameters  $K_f$  and  $1/n$  represent the equivalent of  $K_d$  and the exponent of the equilibrium concentration, respectively ( $1/n$  is 1, by definition, for the linear isotherm). The Freundlich isotherm applies very well to solids with heterogeneous surface properties because the  $1/n$  term takes into account that different sites have different binding energies, with molecules being sorbed at the sites with higher binding energies first, and at sites with lower binding energies later.

The linear and Freundlich parameters ( $K_d$  and  $K_f$ , respectively) calculated for Pb sorption on the basalt and breccia sorbents are presented in Table 5. The equilibrium data points used to construct the isotherms were obtained by hand fitting a best-fit curve to the fractional uptake data. Sorption isotherms for Pb contained a minimum of seven points and were constructed for sorption in synthetic groundwater at pH values of 6, 7, 8, and 9. In all cases,  $K_d$  and  $K_f$  estimates were obtained by fitting a least squares line through the collected data points. The resulting  $K_d$  graphs are shown in Figures 16 and 17.

Table 5. Linear and Freundlich isotherm parameters for lead sorption.

Background Electrolyte Used (Synthetic Groundwater or 0.01M NaNO <sub>3</sub> )	pH	Sorbent Type	K (m <sup>3</sup> /g)	K (g/g)(g/m <sup>3</sup> ) <sup>1/n</sup>	1/n (-)
Synthetic Groundwater	6.0	Basalt	2.14x10 <sup>-4</sup>	2.60x10 <sup>-4</sup>	0.77
		Breccia	3.17x10 <sup>-4</sup>	3.19x10 <sup>-4</sup>	0.67
	7.0	Basalt	4.92x10 <sup>-4</sup>	5.75x10 <sup>-4</sup>	0.92
		Breccia	5.8 <sup>7</sup> x10 <sup>-4</sup>	5.25x10 <sup>-4</sup>	0.72
	8.0	Basalt	1.91x10 <sup>-3</sup>	2.28x10 <sup>-3</sup>	1.06
		Breccia	1.66x10 <sup>-3</sup>	2.09x10 <sup>-3</sup>	0.96
	9.0	Basalt	1.59x10 <sup>-2</sup>	8.83x10 <sup>-2</sup>	1.53
		Breccia	1.43x10 <sup>-2</sup>	3.28x10 <sup>-2</sup>	1.32

With respect to Pb sorption, several conclusions can be drawn by inspection of Table 5. First, the values of the isotherm parameters vary by orders of magnitude, a common phenomenon displayed by pH-dependent sorption behavior. In general, both  $K_d$  and  $K_f$  values tend to increase with increasing pH. This is expected because, as discussed earlier, an increase in Pb sorption is due to increased sorption on the amphoteric surface sites or increasing number or size of surface precipitates. Second, the isotherms do not exhibit true linearity as concluded by the fact that the Freundlich exponents are not equal to 1, although the deviation from 1 is occasionally small. Because of the non-linearity of the isotherms, true distribution coefficients cannot be defined for this particular background electrolyte concentration. Observation of the table, however, shows that the Freundlich exponent comes quite close to 1 at pH 8. Because the measured groundwater pH was approximately 8, the determined distribution coefficients may very well accurately describe the migration of the Pb ion in this system. Otherwise, the calculated  $K_f$  and  $1/n$  parameters can be used

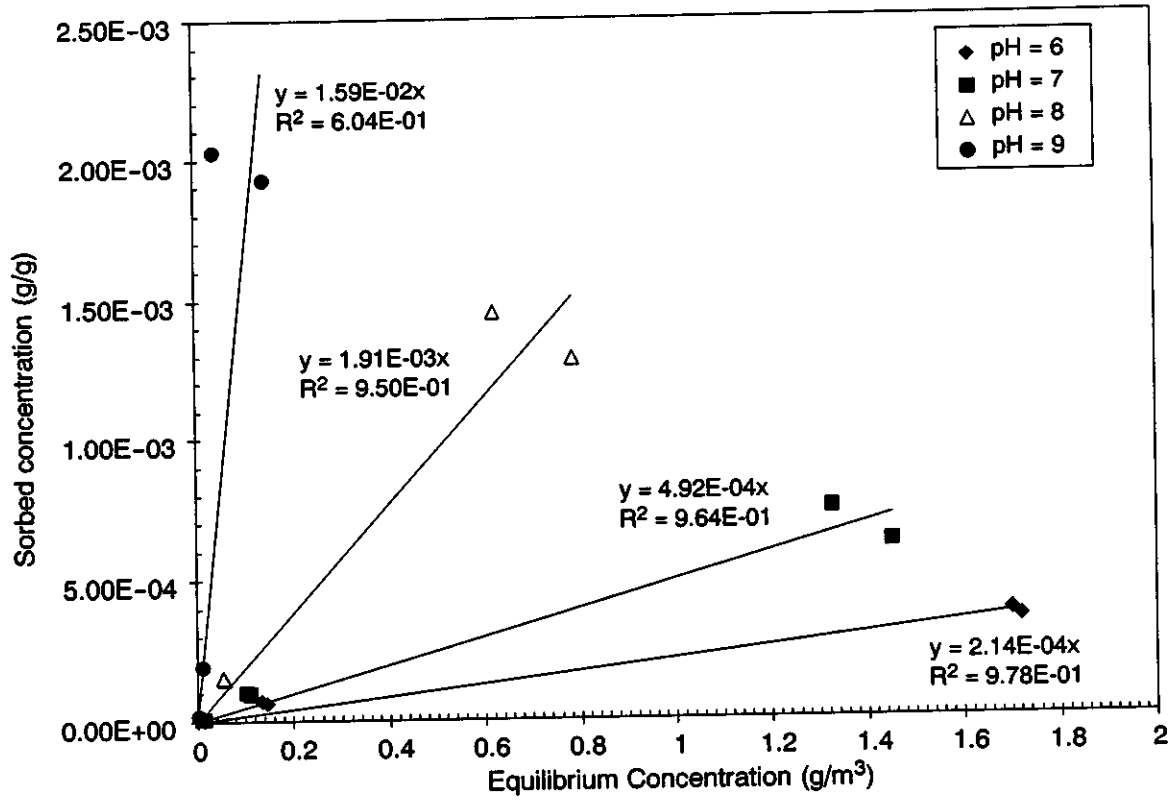


Figure 16. Linear isotherms of  $Pb(NO_3)_2$  sorption on basalt at pH values of 6,7,8, and 9.

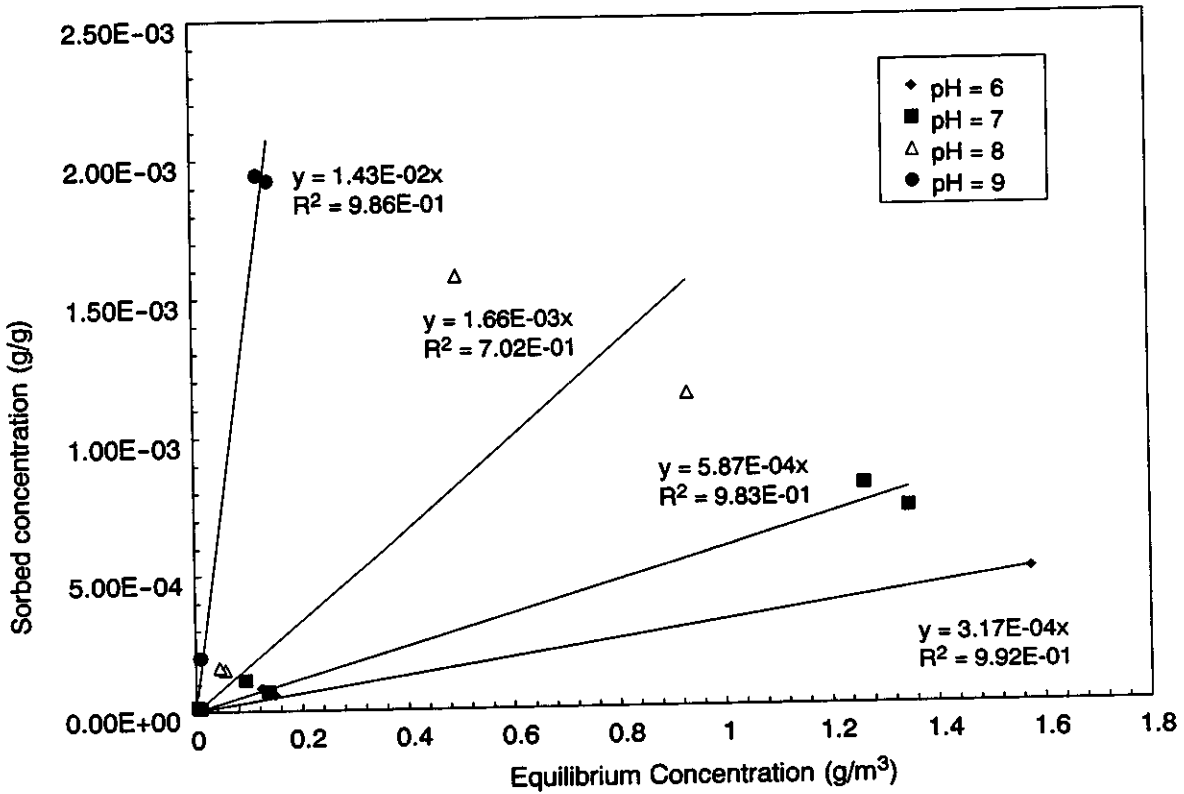


Figure 17. Linear isotherms of  $Pb(NO_3)_2$  sorption on breccia at pH values of 6,7,8, and 9.

as an indication of the sorption capacity of the sorbent for the specific geochemical conditions at which the equilibrium data points were calculated.

Inspection of the table also reveals a trend with respect to the  $1/n$  values, in particular, the values increase with increasing pH. This particular phenomenon indicates that Pb sorption is not occurring in a linear fashion and, as the deviation of the  $1/n$  value from one increases in the positive direction, there is actually an exponential increase in the amount of Pb being sorbed. Again, this may be an indication that Pb is forming precipitates at higher concentrations or pH values.

When comparing the  $K_d$  and  $K_f$  values of the two sorbents, it can also be seen that, at the lower pH values of 6 and 7, both values were higher for the breccia. This is expected because, as previously mentioned, the breccia, having approximately four times the specific surface area of the basalt, had more surface sites available on which sorption could occur. When comparing the  $K_d$  and  $K_f$  values of the two sorbents at the higher pH values of 8 and 9, however, we see that these values are relatively close in most instances, suggesting that there was really no difference in the sorption behavior of Pb on the two sorbents. One possible explanation for this is because at these high pH values, nearly 100 percent sorption occurs on both sorbents resulting in partitioning coefficients that are quite similar.

In conclusion, it appears that the Freundlich isotherm best describes Pb sorption under the circumstances inherent to these experiments. Because the non-linearity of the isotherms is not extremely severe, however, linear distribution coefficients could be used as a starting point for estimating the migration of these ions in the subsurface environment as these are the parameters most commonly incorporated into transport models. Recognition of the limits of the applicability of this approach (concentration range and other experimental variables, however, is necessary before using the simpler linear isotherm, and it is once again noted that using these values beyond the experimental conditions can result in significant errors in sorption behavior prediction.

#### Diffusion of Br through Cannikin Basalt and Breccia

The following section discusses the results of the diffusion experiments performed with the Cannikin Site core samples and provides some background information regarding the underlying theory. A brief summary of the different types of diffusion parameters and how they are estimated is presented first, followed by the experimental results using the Br tracer. Calculations of diffusion coefficients for Pb and Cs are presented subsequently.

#### **Diffusion Parameter Estimation**

Diffusion experiments were conducted using intact pieces of the core samples and a NaBr tracer. The purpose of these experiments was to determine the extent of retardation that was attributable to matrix diffusion. In addition to sorption of solutes at the mineral-water interface, diffusion of ions into the rock matrix serves as an important retardation mechanism by removing ions from the flowing groundwater. Thus, it is important to take diffusion into account so that an accurate estimation of the migration of ions can be attained.

Specifically, the objective of performing the diffusion experiments was to arrive at values describing the diffusion of the Br ion through the core samples, including the effective and apparent diffusion coefficients, and the tortuosity. A brief discussion on each of these parameters and how they are determined is provided below.

The diffusion of ions within the core sample was modeled using the analytical solution of the general diffusion equation:

$$\frac{\partial C}{\partial t} = D \frac{\partial^2 C}{\partial x^2} \quad (6)$$

where  $C$  = concentration of diffusing species in solution (mol/L),  $D$  = diffusion coefficient ( $\text{m}^2/\text{s}$ ),  $t$  = time (s), and  $x$  = distance in the direction of diffusion (m).

The term “diffusion coefficient” in the above equation is used in a general sense and depending on the experimental conditions, it may take different meaning. When describing diffusion of a solute in bulk solution, the diffusion coefficient is referred to as the molecular diffusion coefficient,  $D_{\text{mol}}$ . The molecular diffusion coefficient used in this experiment was determined by the Nernst-Haskell equation (Reid et al., 1977):

$$D_{\text{mol}} = \frac{RT}{F^2} \frac{1/n_+ + 1/n_-}{1/\lambda_+^{\circ} + 1/\lambda_-^{\circ}} \quad (7)$$

where  $D_{\text{mol}}$  = molecular diffusion coefficient ( $\text{m}^2/\text{s}$ ),  $T$  = temperature (K),  $R$  = gas constant (8.314 J/mol-K),  $F$  = Faraday constant (96485 C/mol),  $\lambda_+^{\circ}$ ,  $\lambda_-^{\circ}$  = ionic conductivity at infinite dilution for cation and anion, respectively ( $\text{m}^2\text{S/mol}$ ), and  $n_+$ ,  $n_-$  = valences of cation and anion, respectively (dimensionless).

In porous media, diffusion cannot proceed as fast as it can in a bulk solution because the ions must follow longer pathways as they travel in tortuous paths. To take this into account, an effective diffusion coefficient,  $D_{\text{eff}}$ , is used and is defined as:

$$D_{\text{eff}} = \frac{D_{\text{mol}}}{\chi} \quad (8)$$

where  $\chi$  is the tortuosity (dimensionless), or the actual length of the flow path divided by the straight-line distance between the ends of the flow path of the diffusing species (Hershey and Howcroft, 1998; Fetter, 1994). The tortuosity factor (which accounts for pore structure effects on the length of the diffusion path) incorporates the effects of parameters such as particle size, porosity, and pore size distribution and has typical values ranging from approximately 1.5 to 10 (Papelis et al., 1995). The  $D_{\text{eff}}$  was determined by an analytical approach as described in the following section. Because there is no a priori method for tortuosity estimation, this value was estimated from Equation 8.

If while flowing through the porous medium, the ions are sorbed onto the mineral surfaces or undergo any other reaction(s), the net rate of diffusion will obviously be reduced compared to that for nonsorbing species. In this case, the term *apparent diffusion coefficient*,  $D_{\text{app}}$ , is used to describe the diffusion of the solutes and is defined as:

$$D_{\text{app}} = \frac{D_{\text{mol}}}{\chi \left( 1 + \frac{\rho_b K_d}{\epsilon} \right)} \quad (9)$$

where  $D_{\text{app}}$  = apparent diffusion coefficient ( $\text{m}^2/\text{s}$ ),  $D_{\text{mol}}$  = molecular diffusion coefficient ( $\text{m}^2/\text{s}$ ),  $\chi$  = tortuosity (dimensionless),  $\rho_b$  = solid bulk density ( $\text{kg}/\text{m}^3$ ),  $K_d$  = distribution coefficient ( $\text{m}^3/\text{kg}$ ), and  $\epsilon$  = porosity (dimensionless).

The apparent diffusion coefficient is a function of the solid structure, specifically its density, porosity, and tortuosity, and the specific sorbate-sorbent interactions. The distribution coefficient,  $K_d$  can be estimated from batch equilibrium experiments. It should be noted here, however, that the use of Equation 9 assumes a linear distribution coefficient,  $K_d$  and that, if such a value is not valid based on batch experiments, alternate methods would need to be employed.

It should also be noted here that the diffusion model requires the use of prescribed initial and time invariant boundary conditions (initial solute concentrations at  $t = 0$ ,  $C_o$ , and the final solute concentration at equilibrium  $C_\infty$ ). Likewise, the diffusion was modeled assuming diffusion of fixed initial solute concentration out of the solid core into a well-stirred reactor of limited volume. The solution to Equation 6 would vary depending upon whether nonreactive and reactive solutes were being used due to sorption processes that may affect the latter. The solution for the case of a nonreactive tracer (Br) is presented below.

### Solution to the Diffusion Equation for Nonreactive Solutes

In the case of a nonreactive solute, and taking into account flow through a porous medium, the general diffusion equation becomes

$$\frac{\partial C}{\partial t} = D_{eff} \frac{\partial^2 C}{\partial x^2} \quad (10)$$

where all parameters are as defined in Equation 6. The solution to this equation (assuming no sorption and an independence of  $D_{eff}$  with concentration) is given by Crank (1975) as:

$$C = C_o \operatorname{erft} \left[ \frac{x}{2 \sqrt{D_{eff} t}} \right] \quad (11)$$

where  $\operatorname{erft}$  is the error function,  $C = C_o$  at  $t = 0$  for  $x < a$ ;  $C = 0$  at  $t = 0$  for  $x > a$ ; and  $a$  is the length of the core. Taking the partial derivative, evaluating  $\partial C / \partial x$  @  $x = 0$  and simplifying this equation gives (Hershey and Howcroft, 1998):

$$C_{res} = \left( \frac{2A_{core}}{V_{res}} \right) \frac{C_o \epsilon \sqrt{D_{eff}}}{\sqrt{\pi}} t^{1/2} \quad (12)$$

where  $C_{res}$  = solute concentration in reservoir (mol/L),  $C_o$  = initial solute concentration of saturated core sample (mol/L),  $A_{core}$  = cross-sectional area of the core ( $\text{cm}^2$ ),  $V_{res}$  = volume of the reservoir ( $\text{cm}^3$ ),  $\epsilon$  = porosity (dimensionless),  $D_{eff}$  = effective diffusion coefficient ( $\text{m}^2/\text{s}$ ), and  $t$  = time (s).

By plotting  $C_{res}$  vs.  $t^{1/2}$  and estimating the slope,  $m$ ,  $D_{eff}$  can be calculated by:

$$\frac{C_{res}}{t^{1/2}} = m = \left( \frac{2A_{core}}{V_{res}} \right) \frac{C_o \epsilon \sqrt{D_{eff}}}{\sqrt{\pi}} \quad (13)$$

and rearranging to get:

$$D_{eff} = \left[ \left( \frac{V_{res}}{2A_{core}} \right) \frac{m \sqrt{\pi}}{nC_o} \right]^2 \quad (14)$$

This solution was used to determine the  $D_{eff}$ 's for Br through the basalt and breccia core samples. Once the  $D_{eff}$  was computed for each case, the tortuosity was then calculated using Equation 8. By combining the  $D_{eff}$ , and the  $K_d$  values determined from the batch equilibrium experiments for Pb and Cs,  $D_{app}$ 's were calculated for the reactive solutes.

### Bromide Diffusion

The results of the diffusion experiments showed two trends. First, the estimated diffusion coefficients varied significantly for the two sorbents. Second, the extent of diffusion and the resulting diffusion coefficient varied with time. Each of these findings is discussed in further detail below.

Diffusion of Br out of the basalt sample as a function of time is shown in Figure 18. As expected, the amount of Br in the reservoir increases with time as more Br diffuses out of the core. In the beginning, however, the steep increase in slope indicates that Br is diffusing out of the core rather quickly. This behavior is expected as the pores in closer contact with the reservoir solution (and hence having a shorter travel distance) release the bromide within them. As the duration of the experiment increases, the rate of concentration change decreases, indicating the system is approaching equilibrium. Though Br may still indeed be diffusing out of the core, it is not occurring as quickly as in the beginning of the experiment because the driving force is decreasing (i.e., there is a smaller difference in Br concentration between the core and the reservoir).

The same general behavior was observed for diffusion of Br out of the breccia samples, as can be seen in Figure 19. Again, we see the increase in Br concentration as a function of time as additional Br diffuses out of the core. To estimate the diffusion coefficients, a plot of concentration (mg/L) versus  $time^{-1/2}$  is required. From this plot, the slope of the best-fit line as determined from regression analysis is then used to determine the  $D_{eff}$  as described by Equation 14. Figures 20 and 21 show these plots for each sorbent and the corresponding equations of the best-fit lines.

Table 6 lists the resulting effective diffusion coefficients and tortuosities determined for each sorbent type as a function of the duration of the experiment. As previously mentioned, two trends can be seen from the data: (1)  $D_{eff}$  decreases and tortuosity increases with time, and (2)  $D_{eff}$  for the basalt are smaller than those for the breccia.

Table 6. Diffusion parameters for Br tracer through basalt breccia.

Sorbent Type	Duration of Experiments (days)	Deff (m <sup>2</sup> /sec)	Tortuosity (-)
Basalt	40	5.56x10 <sup>-10</sup>	2.92
	122	1.72x10 <sup>-10</sup>	9.43
Breccia	42	9.23x10 <sup>-10</sup>	1.76
	126	3.58x10 <sup>-10</sup>	4.54

The fact that the tortuosity increased with time is somewhat expected and can be explained as follows. The longer the experiment was allowed to run, the greater the distance Br would have to

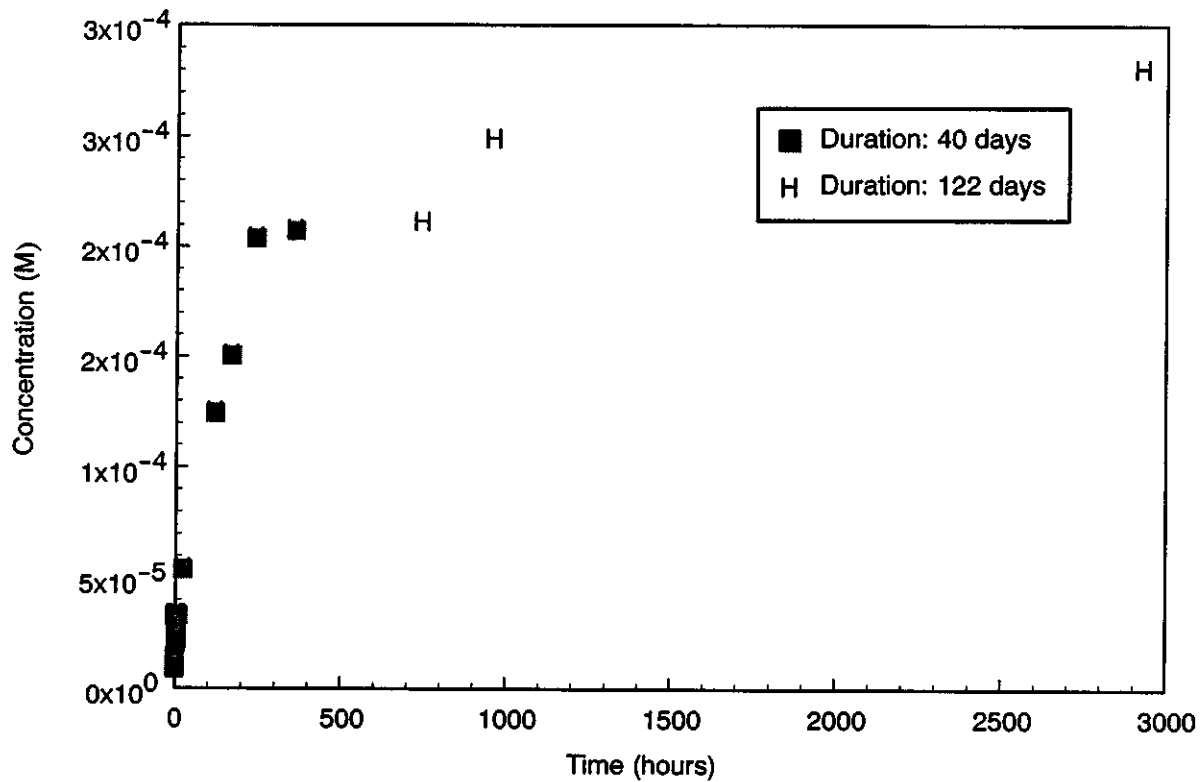


Figure 18. Diffusion of Br out of basalt core sample as a function of time.

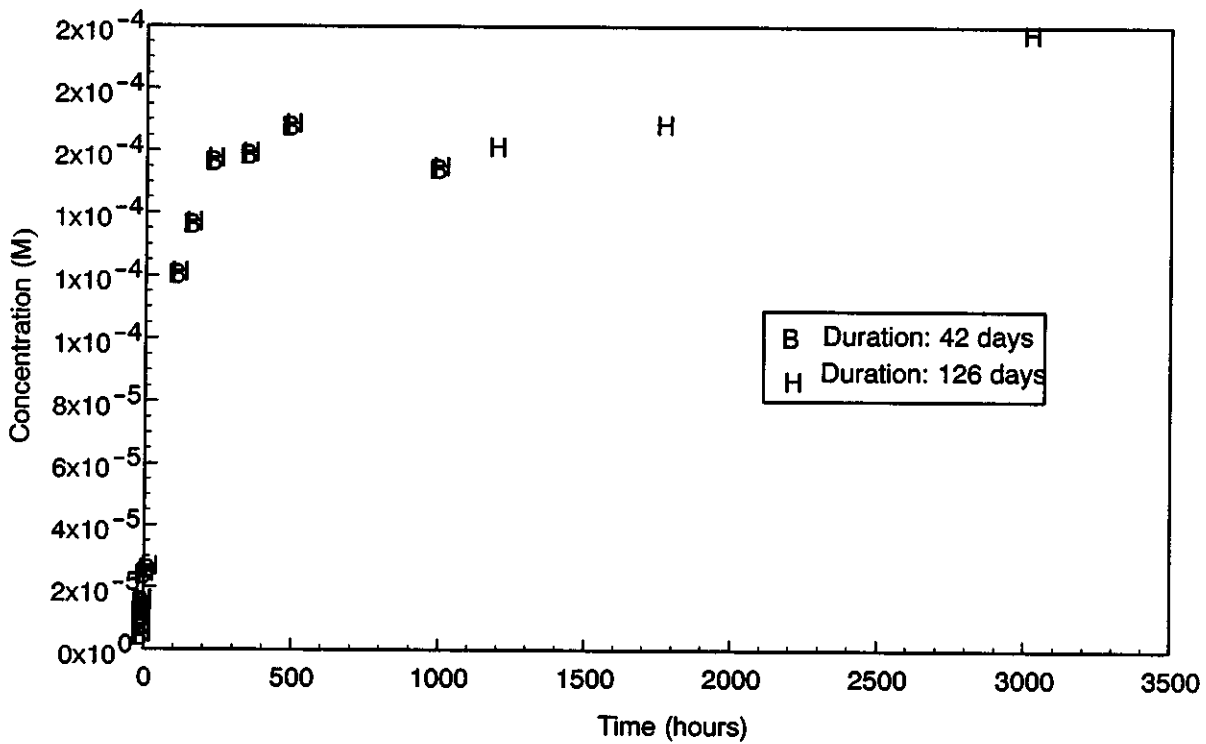


Figure 19. Diffusion of Br out of breccia core sample as a function of time.

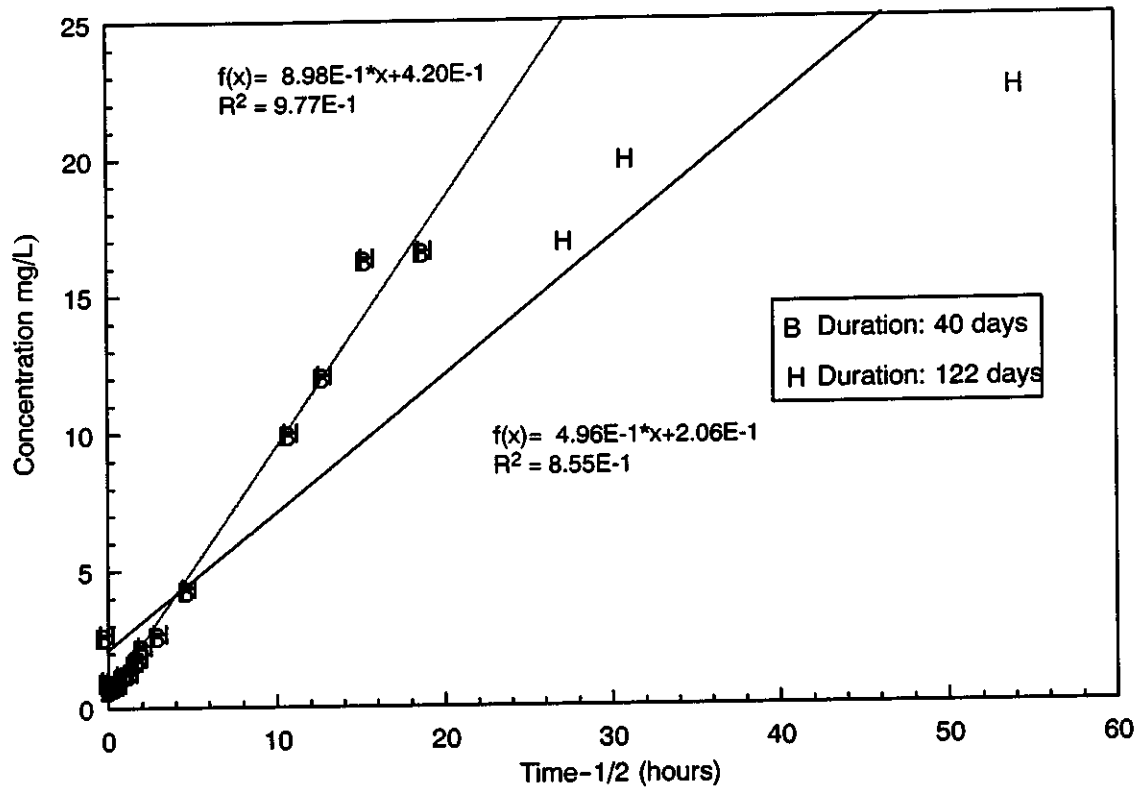


Figure 20. Plot of experimental results and linear regression line of Br diffusion through basalt core.

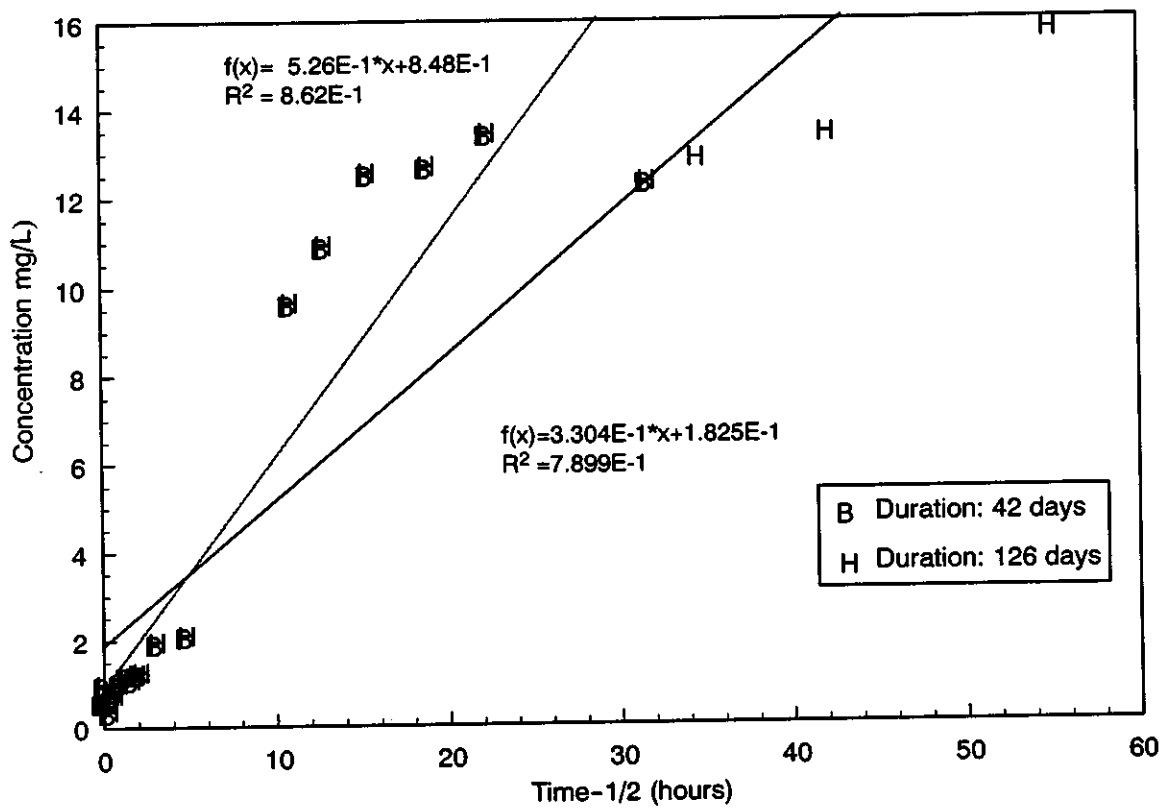


Figure 21. Plot of experimental results and linear regression line of Br diffusion through breccia core.

travel to reach the reservoir solution, i.e., the longer the paths within the core sample would be. Thus, Br diffusing from longer, more tortuous paths would require longer travel times to arrive at the outlet. The porosity of the sample would also play a role in that, a material having a large porosity, would be able to transmit ions in solution more easily. The fact that the breccia had the higher porosity and lower tortuosity demonstrates this point quite well.

It can be seen from the table that, for each duration, the basalt had the lower effective diffusion coefficient between the two sorbent types. Thus, on average, it is expected that a diffusing Br ion would take longer to travel through the basalt compared to the breccia. This is consistent with the fact that the basalt does have the lower surface area and the lower porosity, both of which are factors in transmitting ions in solution.

### **Diffusion Coefficients for Pb and Cs**

With the data provided from the equilibrium sorption and the diffusion experiments, it is possible to estimate an apparent diffusion coefficient for Pb through the use of Equation 9. It is important to note here that, because each  $K_d$  value calculated for Pb is dependent upon pH, the resulting  $D_{app}$  values will be pH-specific as well. The results of these calculations can be seen in Table 7.

As can be seen from the table  $D_{app}$  values range from  $4.72 \times 10^{-16} \text{ m}^2/\text{s}$  to  $1.13 \times 10^{-13} \text{ m}^2/\text{s}$  for the basalt and from  $1.34 \times 10^{-15} \text{ m}^2/\text{s}$  to  $1.62 \times 10^{-13} \text{ m}^2/\text{s}$  for the breccia, depending on pH and reaction time used. From these data, we can conclude that Pb in solution would travel faster through the breccia than through the basalt. This is consistent with the results of the Br experiments in which Br appeared to have diffused through the breccia core more quickly than through the basalt core. One might expect Pb to travel faster through the basalt as the extent of retardation due to sorption on this material is less (as determined through the lower  $K_d$  value). Inspection of Equation 9, however, reveals that the  $D_{app}$  is a function of several factors in addition to the linear distribution coefficient, including the  $D_{mol}$ , tortuosity, bulk density, and porosity. Thus, the fact that the basalt had the higher tortuosity, bulk density, and lower porosity is consistent with the finding that the Pb ion diffused slower through this material.

Table 7. Estimated  $D_{app}$  for Pb diffusion in basalt and breccia.

Sorbent Type	Duration (days)	pH	$K_d$ ( $m^3/kg$ )	$\chi$	D ( $m^2/s$ )
Basalt Porosity = 0.11 Bulk density = 2210 $kg/m^3$	40	6	0.214	2.92	1.13E-13
		7	0.492	2.92	4.93E-14
		8	1.91	2.92	1.27E-14
		9	15.9	2.92	1.52E-15
	122	6	0.214	9.43	3.51E-14
		7	0.492	9.43	1.53E-14
		8	1.91	9.43	3.93E-15
		9	15.9	9.43	4.72E-16
Breccia Porosity = 0.13 Bulk density = 2130 $kg/m^3$	40	6	0.305	1.76	1.62E-13
		7	0.573	1.76	8.60E-14
		8	1.52	1.76	3.24E-14
		9	14.3	1.76	3.45E-15
	122	6	0.305	4.54	6.27E-14
		7	0.573	4.54	3.34E-14
		8	1.52	4.54	1.26E-14
		9	14.3	4.54	1.34E-15

Note:  $D_{mol} = 1.422E-09$ .

Because no sorption of Cs occurred when simulating field conditions (i.e. synthetic groundwater), Cs is expected to act essentially as a nonreactive species and hence only an effective diffusion coefficient can be calculated using Equations 7 and 8. The results of these calculations can be seen in Table 8. Inspection of the table again shows Cs is expected to travel more quickly through the breccia than through the basalt for the same reasons as stated earlier in the discussion regarding diffusion of Br through the samples.

Table 8. Estimated  $D_{eff}$  for Cs diffusion in basalt and breccia.

Sorbent Type	Duration (days)	$\chi$	$D_{mol}$ ( $m^2/s$ )	$D_{eff}$ ( $m^2/s$ )
Basalt	40	2.92	1.98E-09	6.77E-10
	122	9.43	1.98E-09	2.10E-10
Breccia	42	1.87	1.98E-09	1.12E-09
	122	4.54	1.98E-09	4.35E-10

## SUMMARY, CONCLUSIONS, AND RECOMMENDATIONS

During the period of nuclear weapons production and testing, the United States government conducted a series of nuclear weapons tests at various sites throughout the United States and its territories. These tests resulted in subsurface contamination from contaminants such as radionuclides (eg. the cesium radionuclide,  $^{137}Cs$ ), organic compounds, toxic metals (such as lead, Pb), hydrocarbons, drilling mud and residues from plastics, epoxies, and drilling instrumentation (U.S. DOE, 1996). Because of their toxicity or radioactivity, many of these contaminants are considered to be major health hazards and consequently pose a threat to organisms which are

exposed to them. The fate and transport of dissolved contaminants are largely determined by the degree of contaminant interaction with the soil matrix. Studies have shown both, sorption of these ions at the solid-water interface, and diffusion through the porous matrix to be two important factors that may serve as retardation mechanisms.

The objective of this project component was to estimate the rate of migration of reactive (Pb and Cs) and nonreactive (Br) solutes (representative of inorganic contaminants found at underground nuclear test sites) through volcanic basalt and breccia from the Cannikin Test Site, Amchitka Island, Alaska. This site hosted an underground nuclear test conducted in November, 1971. Batch equilibrium sorption and diffusion experiments were performed to estimate isotherm parameters (linear and Freundlich) and diffusion (effective and apparent) coefficients.

The two sorbents used in this study were basalt and breccia. An extensive characterization was performed on each of these sorbents which included mineralogy (solid structure), as determined by x-ray diffraction (XRD), soil pH measurement, major and trace element analysis by x-ray fluorescence (XRF), solid morphology and composition as determined by scanning electron microscopy (SEM) and energy dispersive x-ray (EDX) spectroscopy, respectively, pore size distribution, surface area, porosity and density determination, and cation exchange capacity (CEC).

Sorption experiments were conducted in synthetic groundwater which had an ionic strength of approximately 0.5 M. Because Cs showed no sorption at this high ionic strength, additional experiments were conducted in 0.01 M NaNO<sub>3</sub>.

Lead displayed a typical cation sorption behavior (on amphoteric surface sites) with fractional uptake increasing with increasing pH, despite the high ionic strength of the synthetic groundwater solution used in these experiments. The fact that Pb was able to sorb in such a high ionic strength solution indicates the formation of strong, inner-sphere coordination complexes on these mineral surfaces. Sorption experiments using the high ionic strength synthetic groundwater resulted in no appreciable Cs sorption. It is thus expected that under these conditions, Cs would be highly mobile and exhibit no significant sorption on the solid materials. At the lower ionic strength, however, Cs was able to sorb and demonstrated a sorption behavior that was weakly influenced by pH. Such behavior suggests that sorption of Cs by both sorbents is primarily controlled by sorption on the internal, permanent-charge, cation-exchange sites. The dependence of Cs sorption on ionic strength is a good indication that it is forming outer-sphere ion pair complexes, as expected for an alkali metal.

Based on the experimental data, linear and Freundlich isotherm parameters ( $K_d$  and  $K_f$ , respectively) were calculated for Pb sorption on the basalt and breccia sorbents. The results indicate that equilibrium partitioning at the solid-water interface is strongly pH-dependent for Pb. As a consequence, realistic modeling of the transport of Pb in the system would require knowledge of, or assumptions about, the groundwater pH. No parameters were calculated for Cs because of its inability to sorb under field conditions.

The degree of linearity of the isotherms also varied as a function of pH. It was determined (by inspection of the Freundlich exponent) that the isotherm most closely resembled a linear isotherm at a pH of approximately 8. Because the pH of the synthetic groundwater was determined to be approximately 8, the use of linear distribution coefficients may accurately model the migration of Pb through the system.

The results of the diffusion experiments using a sodium bromide (NaBr) tracer showed two particular trends. First, the estimated diffusion coefficients varied significantly for the two sorbents.

Second, the extent of diffusion and the resulting diffusion coefficient varied with time. It was found that, the basalt sample generally had a lower effective diffusion coefficient than the breccia when comparing the values after approximately equal times of duration. Thus, it is expected that ions traveling through the basalt would move slower than if traveling through the breccia.

Apparent diffusion coefficients were estimated for Pb diffusion through each sorbent. Like the  $D_{\text{eff}}$  using the Br tracer, the  $D_{\text{app}}$  using Pb was lower for the basalt sorbent. This is somewhat expected as the basalt does have a smaller porosity and specific surface area, and a larger bulk density, all of which play a role in the diffusion of ions through the material. Thus, although sorption of Pb was stronger on the breccia, it is generally expected that the retardation of Pb by diffusion through the porous matrix would be greater for the basalt sorbent.

Finally, effective diffusion coefficients were calculated for Cs diffusion through each sorbent. Although Cs is a reactive solute, under the conditions of this experiment it was unable to sorb due to the high ionic strength of the synthetic groundwater. Thus, only a  $D_{\text{eff}}$  was estimated. The results again showed Cs would travel slower through the basalt sample as indicated by the lower  $D_{\text{eff}}$ .

The parameters determined in this study can be used to reduce the uncertainty in radionuclide transport modeling by accounting for retardation of such contaminants due to sorption at the solid-water interface and matrix diffusion. In order to obtain more accurate estimates of the diffusion coefficients, additional diffusion experiments using Pb and Cs as tracers would allow the evaluation of ion-specific effects. Finally, it cannot be overemphasized that the results presented here are specific to the conditions used and that application of the reported parameters to other systems might result in significant errors.

## REFERENCES

- Barnhisel, R.I. and P.M. Bertsch. Chlorites and Hydroxy-Interlayered Vermiculite and Smectite. in *Minerals in Soil Environments*. 2nd ed. (Co-edited by J.B. Dixon and S.B. Weed, eds.). Madison, WI: Soil Science Society of America. (1989): 729-789.
- Blatt, H. and R.J. Tracy. *Petrology: Igneous, Sedimentary, and Metamorphic*. 2<sup>nd</sup> ed. New York: W.H. Freeman. (1996): 529 pp.
- Brown, G.M. Mineralogy of Basaltic Rocks. in *Basalts: The Poldervaart Treatise on Rocks of Basaltic Composition* (Edited by H.H. Hess and A. Poldervaart). New York: John Wiley & Sons. (1967): 103-162.
- Brunauer, S., Emmett, P.H., and E. Teller. Adsorption of Gases in Multimolecular Layers. *J. Am. Chem. Soc.* 60 (1938): 309-363.
- Busenberg, E. and C.V. Clemency. Determination of Cation Exchange Capacity of Clays and Soils Using an Ammonia Electrode. *Clays and Clay Minerals* 21 (1973): 213-217.
- Cox, P.A. *The Elements on Earth*. New York: Oxford University Press. (1995): 113-189.
- Crank, J. *The Mathematics of Diffusion*. 2<sup>nd</sup> ed. Oxford University Press, London. (1975): 414 pp.
- Drever, J.I. *The Geochemistry of Natural Waters: Surface and Groundwater Environments*. 3<sup>rd</sup> ed. Upper Saddle River, NJ: Prentice Hall. (1997): 436 pp.

- Emsley, J. *The Elements*. New York: Oxford University Press. (1989): 256 pp.
- Fetter, C.W. *Applied Hydrogeology*, 3<sup>rd</sup> ed. Englewood Cliffs, NJ: Prentice Hall. (1994): 691 pp.
- Freeze, R.A. and J.A. Cherry. *Groundwater*. Englewood Cliffs, NJ: Prentice Hall. (1979): 604 pp.
- Gottardi, G. and E. Galli. *Natural Zeolites*. New York: Springer-Verlag. (1985): 409 pp.
- Greenwood, N.N. and A. Earnshaw. *Chemistry of the Elements*. Tarrytown, NY: Pergamon Press. (1984): 1543 pp.
- Gregg, S.J. and K.S.W. Sing. *Adsorption, Surface Area, and Porosity*. 2nd ed. Orlando, FL: Academic Press, Inc. (1982): 303 pp.
- Hammond, C.R. The Elements. in *CRC Handbook of Chemistry and Physics*. 80th ed. (David R. Lide, Editor in Chief). New York, NY: CRC Press. (1995): 4.1-4.34.
- Hart, W.A. et al. The Chemistry of Lithium, Sodium, Potassium, Rubidium, Cesium, and Francium. in *McGraw-Hill Encyclopedia of Chemistry*. 2nd ed. (S.P. Parker, Ed.). New York, NY: McGraw-Hill, Inc. (1992): 1236 pp.
- Hershey, R.L. and W.D. Howcroft. "Results of Laboratory Experiments Measuring the Tortuosity of Granite from the Shoal Site, Nevada. *Desert Research Institute Report*. (1998): 9 pp.
- Huang, P.M. Feldspars, Olivines, Pyroxenes, and Amphiboles. in *Minerals in Soil Environments*. 2nd ed. (Co-edited by J.B. Dixon and S.B. Weed). Madison, WI: Soil Science Society of America. (1989): 975-1051
- Jackson, J.A. *Glossary of Geology*. 4<sup>th</sup> ed. Alexandria, Virginia: American Geological Institute. (1997): 769 pp.
- Knox, R.C., Sabatini, D.A. and L.W. Canter. *Subsurface Transport and Fate Processes*. Boca Raton, FL: Lewis Publishers. (1993): 430 pp.
- Lee, W.H. and L.M. Gard. Summary of the Subsurface Geology of the Cannikin Site, Amchitka Island, Alaska. *United States Department of the Interior Geological Survey Report #USGS-474-132*. (1971): 24 pp.
- LeMaitre, R.W. "Some Problems of the projection of chemical data into mineralogical classifications. *Contrib. Mineral. Petrol.*, 56 (1976): 181-189.
- Ming, D.W. and F.A. Mumpton. Zeolites in Soils. in *Minerals in Soil Environments*. 2nd ed. (J.B. Dixon and S.B. Weed, eds.). Madison, WI: Soil Science Society of America. (1989): 873-911.
- Morel, F.M. and J.G. Hering. *Principles and Applications of Aquatic Chemistry*. New York: John Wiley & Sons, Inc. (1993): 588 pp.
- Mumpton, F.A. Natural Zeolites. in *Mineralogy and Geology of Natural Zeolites*. (Edited by F.A. Mumpton). Reviews in Mineralogy 4. Chelseas, MI: Mineralogical Society of America. (1981): 1-17.
- Papelis, C and D.A. Sloop. Equilibrium Studies of Lead, Cesium, Strontium, Chromate, and Selenite Sorption on Granite from the Project Shoal Test Site, Fallon, Nevada. *Desert Research Institute Report*. (1997): 51 pp.

- Papelis, C., Equilibrium Studies of Lead, Strontium, Chromate, and Selenite Sorption on Granite from the Project Shoal Test Site, Fallon, Nevada. *Desert Research Institute Report*. (1997): 24 pp.
- \_\_\_\_\_. Evaluation of Cobalt Mobility in Soils from the Nevada Test Site. *Desert Research Institute Report*, (1996): 40 pp.
- \_\_\_\_\_. P. Roberts, and J. Leckie. Modeling the Rate of Cadmium and Selenite Adsorption on Micro- and Mesoporous Transition Aluminas. *Environmental Science & Technology* 29, no. 4 (1995): 1099-1108.
- Reid, R.C., J.M. Prausnitz, and T.K. Sherwood. *The Properties of Gases and Liquids*. 3<sup>rd</sup> ed. New York, NY: McGraw-Hill. (1977): 688 pp.
- Ruthven, D.M. *Principles of Adsorption and Adsorption Processes*. New York: John Wiley & Sons. (1984): 433 pp.
- Stumm, W.S. and J.J. Morgan. *Aquatic Chemistry: Chemical Equilibria and Rates in Natural Waters*. New York, NY: John Wiley & Sons. (1996): 1022 pp.
- Travis, C.C. and E.L. Etnier. "A Survey of Sorption Relationships for Reactive Solutes in Soil." *Journal of Environmental Quality* 10, no. 1 (1981): 8-15.
- U.S. Department of Energy, Office of Strategic Planning, 1996, *The 1996 Baseline Environmental Management Report*. Volume II, Alaska-New Jersey. (1996): 484 pp.
- Waldron, H.A., ed. *Metals in the Environment*. San Francisco, CA: Academic Press. (1980): 333 pp.